INVESTIGATION OF ELECTRICAL PROPERTIES OF SURFACE STRUCTURES BY X-RAY PHOTOELECTRON SPECTROSCOPIC TECHNIQUE UNDER EXTERNAL VOLTAGE STIMULI

A THESIS

SUBMITTED TO THE DEPARTMENT OF CHEMISTRY

AND THE INSTITUTE OF ENGINEERING AND SCIENCES

OF BİLKENT UNIVERSITY

IN PARTIAL FULFILLMENT OF THE REQUIREMENTS

FOR THE DEGREE OF

MASTER OF SCIENCE

By

U. KORCAN DEMIROK

February 2005

I

I certify that I have read this thesis and that in my opinion is it is fully adequate, in scope and quality, as a thesis of the degree of Master in Science

……………………………………..

Prof. Dr. Şefik Süzer (Principal Advisor)

I certify that I have read this thesis and that in my opinion is it is fully adequate, in scope and quality, as a thesis of the degree of Master in Science

……………………………………..

Prof. Dr. Abdullah Atalar

I certify that I have read this thesis and that in my opinion is it is fully adequate, in scope and quality, as a thesis of the degree of Master in Science

……………………………………..

Assoc. Prof. Dr. Ömer Dağ

I certify that I have read this thesis and that in my opinion is it is fully adequate, in scope and quality, as a thesis of the degree of Master in Science

……………………………………..
Assoc. Prof. Dr. Margarita Kantcheva

I certify that I have read this thesis and that in my opinion is it is fully adequate, in scope and quality, as a thesis of the degree of Master in Science

……………………………………..
Assoc. Prof. Dr. Ahmet Oral

Approved for the Institute of Engineering and Sciences

……………………………………..
Prof. Dr. Mehmet Baray
Director of Institute of Engineering and Science

ABSTRACT

INVESTIGATION OF ELECTRICAL PROPERTIES OF SURFACE STRUCTURES BY X-RAY PHOTOELECTRON SPECTROSCOPIC TECHNIQUE UNDER EXTERNAL VOLTAGE STIMULI

U. KORCAN DEMİROK

M.S. in Chemistry

Supervisor: Prof. Dr. Şefik Süzer

February, 2005

Electrical properties of surface structures are analyzed using XPS (X-Ray Photoelectron Spectroscopy) by means of external stimuli together with a novel technique allowing the user to record 200 conventional spectra in a period of one second with a time resolution of 5ms.

Charging processes of surface structures such as SiO_2 and C_{12}-thiol-capped gold nanoclusters are monitored by time resolved XPS technique which gives an approximate charging constant of the system (RC), and electrical parameters like resistance and capacitance are estimated using external biasing and other relevant time resolved XPS data. Moreover, development and optimization of the technique are carried out by certain parameters and observing the changes in the time constants and binding energy shifts.

It is also shown that application of positive and negative external bias can be used to identify two different forms of gold that exist together in the same sample, as nanoparticles and bulk metal, by means of stimulating the charging-induced-separation of the Au 4f peaks which would otherwise appear as overlapped photoemission signals in the grounded spectrum.

Keywords: SiO_2/Si, Charging, External Bias, Time Resolved XPS, Time Constant, Gold Nanoparticles

ÖZET

DIŞARIDAN VERİLEN VOLTAJ YARDIMIYLA YÜZEY YAPILARININ ELEKTRİKSEL ÖZELLİKLERİNİN X-IŞINI FOTOELEKTRON SPEKTROSKOPİSİ KULLANILARAK İNCELENMESİ

U. KORCAN DEMİROK
Kimya Yüksek Lisans Tezi
Danışman: Prof. Dr. Şefik Süzer
February 2005

Çeşitli yüzey yapılarının elektriksel özellikleri XPS (X-Işını fotoelektron spektrumu) tekniği ile ve dışarıdan verilen voltaj yardımıyla, bir saniye içinde 5 milisaniye aralıklarla 200 spektrum alınmasına olanak sağlayan ilk kez tarafımızdan geliştirilmiş yeni bir teknikle incelendi.

SiO_2 ve C_{12}-thiol kaplı altın nano-parçacıklarının elektriksel yüklenme süreçleri incelenen sistemin RC sabitinin ölçülmesine olanak tanıyan bu yeni zaman çözünümlü XPS tekniği ile incelendi ve yardımcı başka yöntemler de kullanılarak bu malzemelerin resistans ve kapasitans değerleri tayin edildi.

Bunlarla birlikte bu yeni tekniğin geliştirilmesi ve verimliliğinin arttırılması amacıyla çeşitli parametrelerin değiştirilmesi ve zaman sabitlerine ve bağlanma enerjilerinin kaymalarına etkilerinin gözlenmesi suretiyle çalışmalar yapıldı.

Bunun yanında dışarıdan uygulanan voltajın aynı numune üzerinde bulunan ve topraklanmış XPS spektrumunda üst üste görünen altın metali ve altın nano-parçacıklarından gelen altın 4f sinyallerinin ayrılmasını sağlayabileceği ve neticede bu iki altın şeklinin XPS spektrumunda ayrı ayrı görülebileceği gösterildi.

Anahtar Kelimeler: SiO_2/Si, Yüklenme, Dışarıdan Voltaj Uygulanması, Zaman Çözünümlü XPS, Zaman Sabiti, RC Sabiti, Altın Nano-parçacıkları

ACKNOWLEDGEMENTS

It is more than a pleasure and an honor to overstate my deepest gratitude here to my dear supervisor Prof. Dr. Şefik Süzer. He has not only been a supervisor to me with his vast knowledge and experience throughout my studies, but also a perfect model both as a person and an outstanding academician in the field. I am very lucky that I have been able to learn such virtues from him that I would thank him for years. I deeply appreciate and would like to thank him endlessly for being an instructor, professor, supervisor and an elder of mine.

I would like to extend my kindest gratitude to; Dr. Gülay Ertaş for her company, help and valuable discussions throughout my studies and my very dear friend Burak Ülgüt for his years-long friendship and joyful undergraduate frames that I would not forget. I wish the best for him during all his dear life.

I also would like to thank to former and current Süzer-Lab members; Özgür Birer, Ferdi Karadaş, H. Nezih Türkçü, Ercan Avcı, Ilknur Kaya-Tunç, Bora İnci and Eda Özkaraoğlu for their help and pleasant presence in the lab.

I appreciate the moral support by dear friends; Selim Alayoğlu, Rukiye Karadeniz, Gökhan Arıkan, Ümit Akbal, Anıl Ağıral, A. Faik Demirörs, Nesibe Çındır, Mehtap Küyükoğlu, Oğuzhan Çelebi, Mehmet Göllü, Ethem Anber, Serdar Durdağı, Cenk Tura, Yaşar Akdoğan and Olga Samarskaya.

I am deeply indebted to Bilkent University and the Chemistry Department for providing us such a solid and high-quality education.

Finally, I can not express even a bit of my love and gratitude with strongest words on earth for my very dear mother, father and my dear brother.

TABLE OF CONTENTS

LIST OF TABLES

LIST OF FIGURES

VIII

X

1. INTRODUCTION

1.1. X-ray Photoelectron Spectroscopy (XPS)

XPS (X-ray Photoelectron Spectroscopy) has been one of the leading surface analysis techniques for monitoring surface structures and modifications in the nanometer scale. Based on the photoelectric effect[1,2] XPS was developed in mid-1960's by Kai Siegbahn and his research group at the University of Uppsala, Sweden.[3]

In general use of XPS, binding energies of the electrons that are emitted from different atomic levels of various elements are measured via which all chemical information is derived.[4] Thus, composition of the surfaces, chemical states of the components and charging behavior of the surfaces are obtained through XPS analysis.

1.1.1. Principles
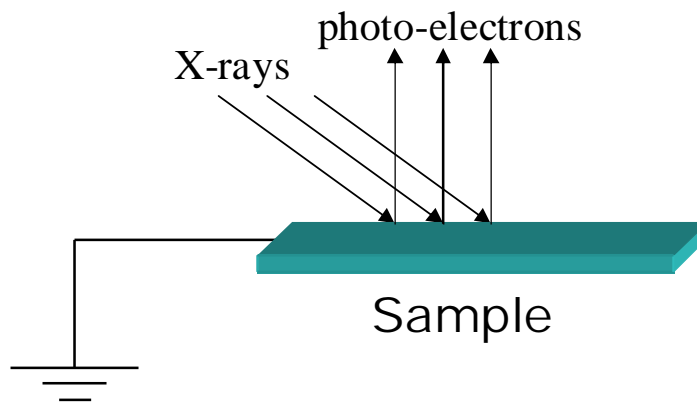
Figure 1. Formation of Photoelectrons

By means of an incident X-ray irradiation which is directed towards the sample, photoelectrons are emitted and kinetic energies of the photoelectrons emitted from the sample are measured in the electron energy analyzer, which, in turn, gives the binding energy

of the corresponding electron. This analysis yields the elemental composition of the outermost layers that are in question.

The X-ray photoemission process is governed by the equation,

$$BE = h\nu - KE - \Phi \qquad (1)$$

where $h\nu$ is the energy of the incident photon, BE is the binding energy, KE is the kinetic energy of the electrons emitted and Φ is the work function of the sample and the instrument.

To a great extent, the electrons detected by the analyzer during a photoemission process are from the outermost layers (<10 nm). Although X-rays can penetrate deeper (~1μm) into the material to create photoelectrons, these electrons can not survive since they lose most of their energies during inelastic collisions throughout the way to the surface of the material. Inelastic mean free path (λ), which is a measure of the distance traveled by a photoelectron inside the sample, is an important indication of the possibility that a given photoelectron can end its trajectory up with the detector[5] and is defined as $I/I_0 = e^{-1}$. The reason why XPS is such a surface sensitive technique is that the electrons, which have enough energy to travel more than 3λ, can reach the analyzer and constitute a signal where λ is in the range between 0.4 nm and 4 nm. Therefore the signals are obtained from the outermost 10-12 nm of the sample in question. However, it is possible to further increase the surface sensitivity by means of Angle Resolved XPS.[6-7]

1.1.2. Applications

XPS can be used for a wide variety of applications; chemical analysis being the most frequently used one.

1.1.2.1. Chemical Analysis

Although the X-ray photoemission process is not as strong as the photoemission process in Ultraviolet Photoelectron Spectroscopy, it is powerful enough for precise analysis at molecular levels regarding chemical compositions of surface structures.

Besides qualitative information obtained by XPS on elemental compositions of substrates analyzed, the relative atomic ratios of the components can also be found by appropriate analysis of the resulting XPS spectrum such that,

$$\frac{X}{Y} = \frac{(A)_X}{(A)_Y} \frac{\sigma_Y}{\sigma_X} \left(\frac{E_K^Y}{E_K^X} \right)^{3/2}$$

(6)

where X/Y is the atomic ratio of species X to species Y in the sample, A is the area of the corresponding peak in the spectrum, σ is the photoionization cross-section and E_K is the kinetic energy of the corresponding peak.

Besides its use in elemental differentiation, XPS also gives information on the chemical state of a particular atom. Since the chemical state of an atom creates a unique potential around the photoelectron ejected, the kinetic energy of the photoelectron in question is affected by the surrounding potential. This increase or decrease in the kinetic energy of the

photoelectron, which is termed as chemical shift, relative to the neutral atom gives information on the chemical state of the atom in question.
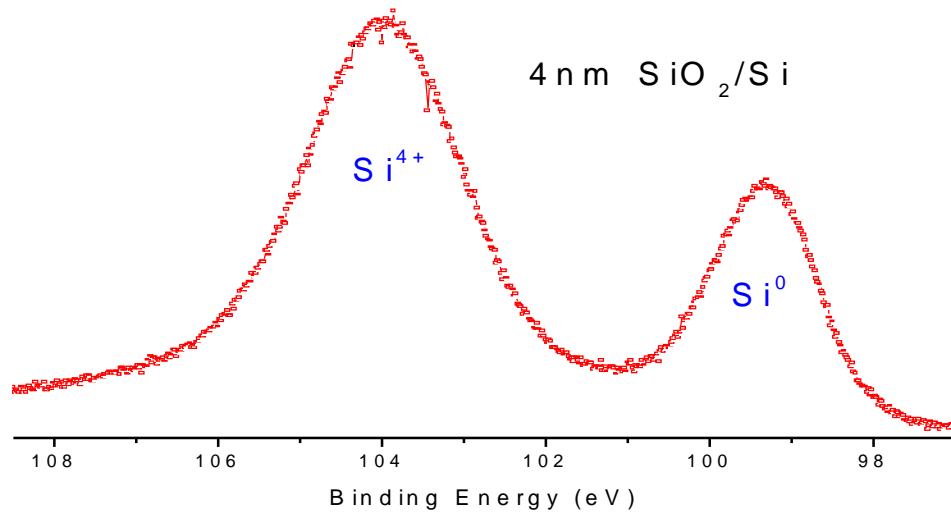
Figure 2. Two different oxidation states of Si in a 4 nm-thick-SiO_2/Si System

In Figure 2, Si in its neutral and 4+ oxidation states are represented by two separated peaks in the spectrum.[8] Due to positive environment around the electron to be ejected by an X-ray in Si^{4+}, photoelectrons from Si^{4+} are shifted towards higher binding energies in the energy scale. Likewise, photoelectrons ejected from a negative environment would produce a shift towards lower binding energy values.
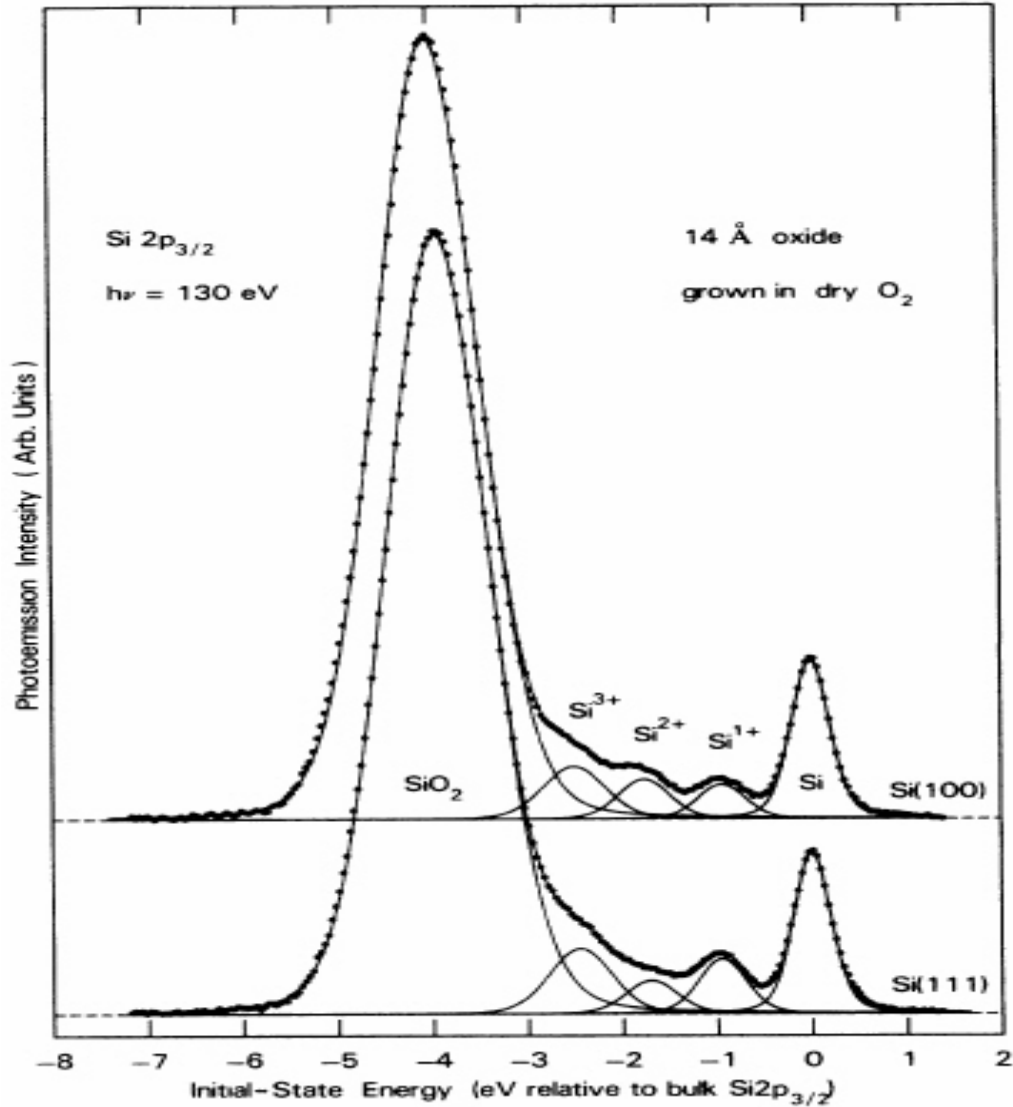
Figure 3. Core level XPS spectra of 1.4nm-thick SiO_2 overlayers on Si (100) and Si (111)

In the work of Himpsel et.al.[9], four different oxidation states of silicon and its neutral form, namely, Si^0, Si^{1+}, Si^{2+}, Si^{3+}, and Si^{4+}, in Si (100) and Si (111) substrates are displayed together in high resolution XPS spectra. The spectrum was recorded at 130eV photon energy which belongs to a 0.5 nm oxide overlayer that was grown in $2x10^{-5}$ Torr at 750^0C to show that interfacial states with different oxidation states exist between the bulk silicon and the

oxide. The relative intensities of these states are shown to be different in Si (100) and Si (111) and are explained by differences in interfacial structures in these two forms. However, the effect of oxygen pressure on the growth of interfacial states and the intensities observed in XPS spectra are shown to be more or less the same for different pressure values between $2x10^{-5}$ Torr to 0.1 Torr. Moreover, the thickness of the oxide film, as in the case of the pressure of oxygen, also does not influence much the relative ratios of energies of +1, +2, +3 states of silicon to Si^0. This was demonstrated by growing a 1.4nm thick oxide layer on both Si (100) and Si (111) substrates at 0.1 Torr O_2. It is also noticed that the energies of the Si2p photoemission coming from +1, +2 and +3 states are closer to Si^0 rather than being evenly distributed between the S^{4+} and Si^0. This shows that although the oxidation states are increased one by one going up from Si^0 to Si^{4+}, the overall potential around these structures is not just determined barely by the oxidation state itself but also by the local environment. The fact that an oxidation state of an atom does not directly refer to its charge transfer properties is in parallel with the above statement. Therefore also adding the enhancement of photoionization cross section of higher-oxidation states into account[9], it can be inferred from the spectra that +1, +2 and +3 states are in a more partially negatively charged medium than the +4 state. The relative binding energies of the interfacial states versus the charge of silicon is plotted in Figure 4. It is seen that up to Si^{4+}, the values show almost a prefect linear dependence with an R^2 value of 0.996 within experimental limits with +4 state slightly being deviated from the derived linear dependence.
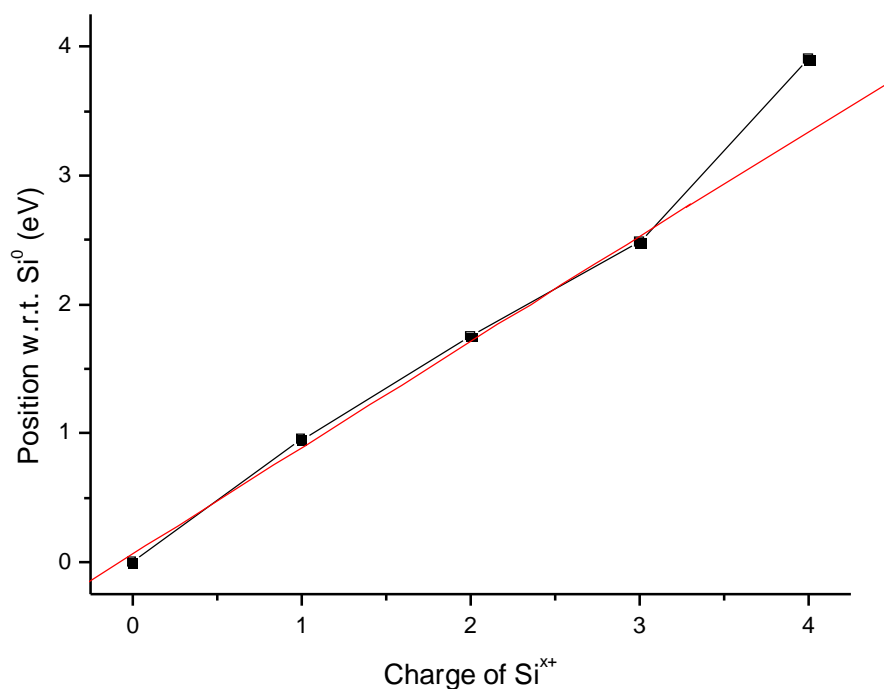
Figure 4. The relative binding energies of the corresponding oxidation states of silicon with respect to silicon in its neutral state

1.1.3. Charging in XPS

In XPS, charging is the phenomena during which a positive charge develops in the substrate under X-ray irradiation due to lag of replenishment of the ejected electrons. In non-conducting samples, as shown in Figure 5, since photoelectrons are emitted faster than the rate of replenishment from the ground, a positively charged environment is created, which in turn affects the binding energy of the ejected photoelectrons. The kinetic energies of the photoelectrons that reach the detector are lowered due to the extra electrostatic attraction that takes place between the electron and its environment during photoemission process. Possible charging behavior is prevented in conducting samples via grounding the sample. In this case,

the emission of a photoelectron is quickly followed by insertion of another electron coming from the ground inside a hole almost immediately ($t<10^{-9}$s).
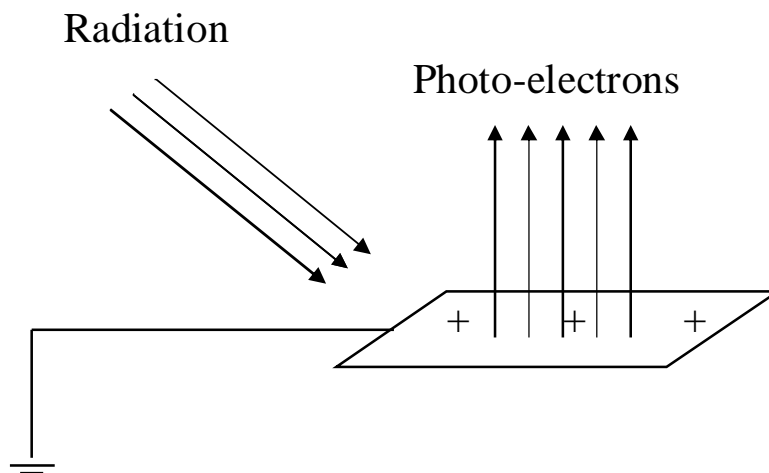
Figure 5. Charging in a non-conducting sample

The charging process can be simulated artificially in a conductor which normally would not charge. Suzer's group has induced positive and negative charging in a gold sample by addition of an external resistor. The sample is then put under a series of positive and negative external voltages to follow the corresponding changes in the Au4f peak maxima. The binding energy differences between the original gold peak and the peak that belongs to gold plus the external resistance are then plotted. As it is also shown below, the binding energy values of Au4f coming from Au+20MΩ system was found to be higher than the original Au4f in the negative bias region (including ground) due to the resistive element in the circuit restricting the movement of electrons and causing the gold to feel and extra positive potential. Likewise the Au+20MΩ system is found at lower binding energies than the original gold in positive bias region which means that the electrons that move from the

8

sample to the source are now slowed down with the resistor causing an extra negative potential around gold.
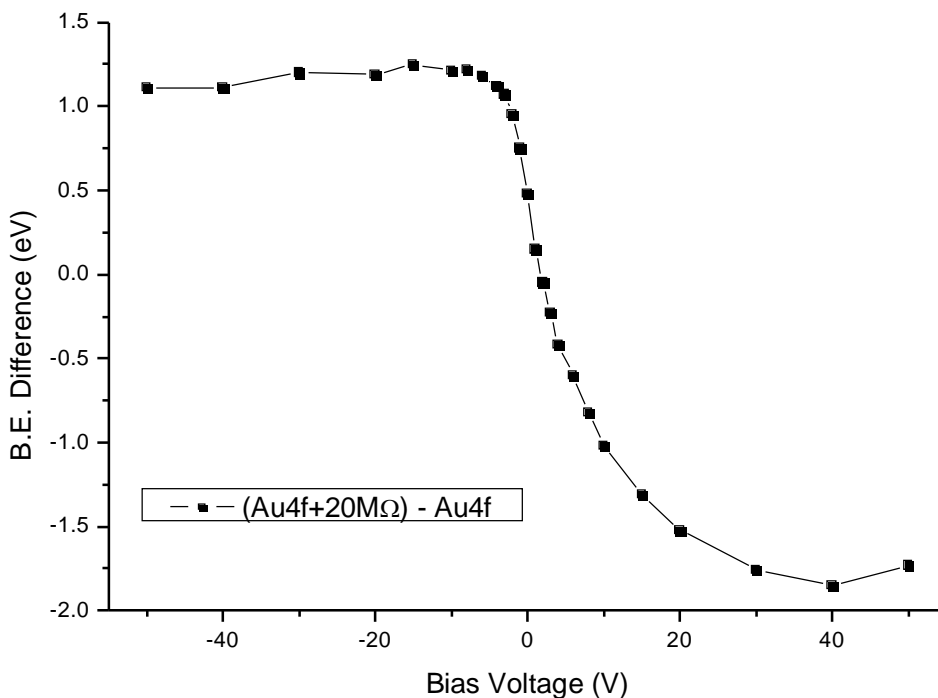
Figure 6. The effect of resistance on the binding energy values of gold.

Although charging has generally been considered as a problem preventing accurate determination of binding energies of various components in non-conducting samples[10,11,12,13], it has also been used as a useful tool for various applications in the case of samples containing heterogeneous surface structures.[14,15,16,17] Differential charging[18,19], which results due to differences in charging behavior of layers/components inside the same medium under same conditions, is also another parameter which has been under extensive investigation. Relative charging differences that exist inside a sample having a varying composition of

different atoms or even among the identical elements in a medium which vary only in their morphology allow the investigator to benefit from this differential charging information.[20,21]

In a recent study by Suzer[21], silicon peaks that belong to a PDMS overlayer deposited on top of a SiO_2 layer are separated, which otherwise would appear as overlapped features, by making use of differential charging. Upon biasing the system at -5V, first spectral features of Si^{x+} coming from PDMS layer are seen by fitting the peaks in the corresponding region of the XPS spectrum. Si2p photoemission coming from PDMS is further separated from the one coming from SiO_2 in the case of -10V negative biasing.

Charging is often handled with referencing and neutralization by low energy electrons. A specific photoelectron peak of known value can be used to calibrate the spectrum. Generally, C1s peak coming from the contamination of a surface or the Au 4f peaks placed in contact with the sample serve as references. The second solution, i.e. neutralizing by electron flood gun, have been extensively used to employ low energy electrons to replenish the ejected photoelectrons.[22,4]

When combined with information derived from differential charging, external basing[8,23], is another important technique in the analysis of surface structures by XPS.

1.2. External Bias Induced Sample Probing with XPS

As mentioned earlier above, external biasing has proven to be a simple yet informative tool[8] in XPS analysis of various surface structures. In general, the sample is biased with a positive or negative D.C. voltage to induce voltage dependent shifts in XPS spectra.
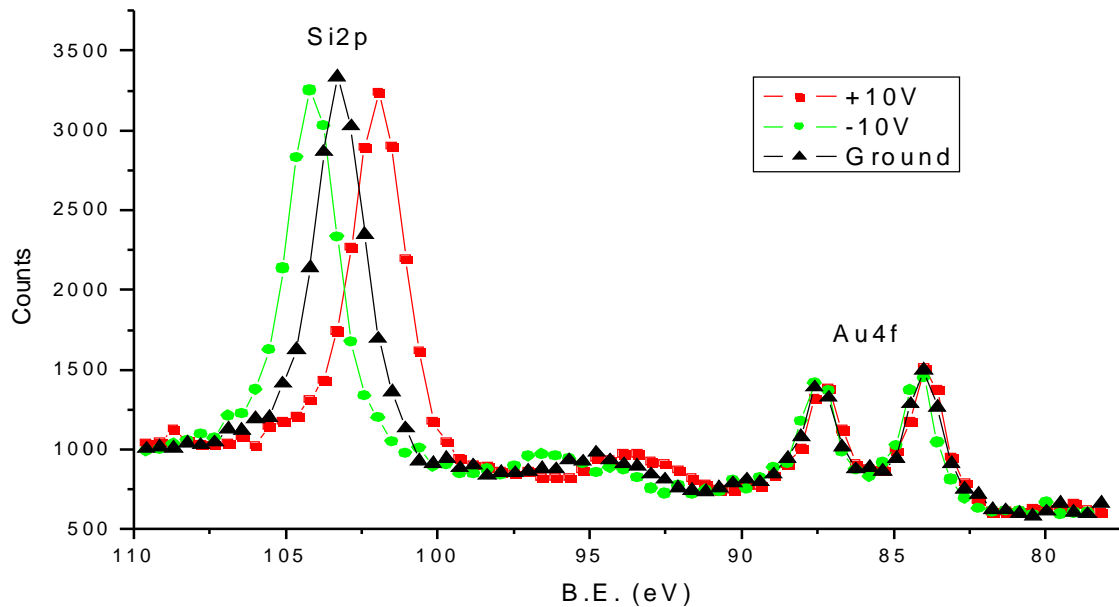
Figure 7. Externally D.C. biased $Si/SiO_2/Au$(foil) System

In Figure 7, a semiconductor/oxide/metal system, i.e. $Si/SiO_2/Au$(foil), is shown, which was put under -10V and +10V external bias, together with a grounded spectrum. Gold 4f peaks were selected as references and Au4f photoemission in all three spectra were superimposed in the same graph. Si2p coming from the bulk Si is not visible since oxide is thick, ca~200 nm.

1.2.1. Effects on Charging

External bias can be useful in understanding the mechanisms involved during the process of surface charging. It is visible from Figure 7 that without exact energy determination, the absolute amounts of positive and negative charging of Si with respect to Au are different from each other meaning that the differential charging of SiO_2 under positive and negative biasing are different in each case, although the absolute value of the voltage

11

applied is the same for both. Peak positions and corresponding differences are illustrated in Table 1.

Voltage	Si 2p Peak Position	Diff. w.r.t Au 4f	Relative Diff.
+10V	101.95eV	17.95eV	1.35eV
G	103.3eV	19.3eV	
-10V	104.2eV	20.2eV	0.9eV

Table 1. Amount of charging in oxide overlayer together with positive and negative

charging with respect to ground.

As it is seen from Table 1 that the Si2p photoemission exhibits a shift of 1.35eV with respect to ground under positive D.C. bias where the shift reduces to 0.9eV displaying a 0.45eV decrease in shifts due to charging when the system is under the negative D.C. biasing. This change in the differences between ground and the corresponding peak positions of positive and negative D.C. bias is attributed to differences in neutralization efficiency of stray electrons in these two cases in one of the detailed studies of Karadas et. al.[23] on differential charging. In the case of negative bias, the stray electrons are repelled by the surface causing the Si2p shift to be greater than in the case of positive bias. However, upon application of positive bias, the stray electrons are attracted to a greater extent to the sample causing an over-neutralization and resulting in a decrease in the shift of Si2p photoemission to relatively a lower binding energy value than the ideal expected shift of +10V.

In addition to the information obtained by external biasing on the nature of charging in various systems, one can use external biasing to deduce other useful chemical or structural information. In one previous application of external bias Havercroft et al. reported that they have been able to use negative external bias to identify chemical differences in oxide films on an aluminum alloy.[24] In another study[25], we applied positive and negative external bias to separate the photoemission peaks of two different forms of gold, i.e. bulk and capped nanoparticles, which would otherwise be seen as overlapped features in the case of conventionally grounded sample probing. The details of this work will be discussed later in this text.

1.3. Time-Dependent XPS measurements

XPS is generally used to extract chemical information from the sample on its composition or other parameters which does not vary in time. The main reason for this type of 'restricted' use is due to the complexity and difficulty of probing dynamic systems which are far from equilibrium. Moreover, the average period that one can obtain decent spectrum is of the order of minutes. Therefore XPS is seldom used to probe fast processes on surfaces.

What is generally meant up to this thesis work by time-dependent or time-resolved XPS is merely the acquisition of consecutive several-minute-long XPS spectra one after another, taking minutes, hours, or days to complete, for monitoring the changes that take place on the surface.[26] One example to these 'time-resolved' measurements is the work by Deng et. al.[27], in which GaAs(100) and InP(100) samples were cleaved in UHV to have (110) surfaces. Upon this cleavage the energy band changes in these samples were studied in a timely manner by high resolution XPS.
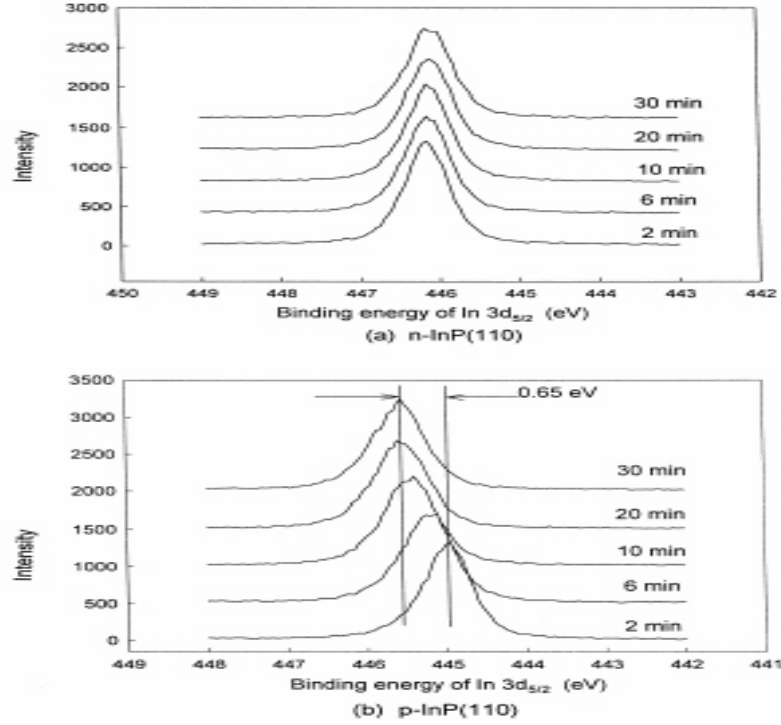
Figure 8. Time-resolved XPS spectra of In $3d_{5/2}$ of a) n-InP(110) and b) p-InP(110) after cleaved in UHV[27]

Consecutive XPS spectra of In $3d_{5/2}$ photoemission from n- and p-InP(110) is displayed above to show the changes that occur in the peak position of In $3d_{5/2}$ in time. A minimum period of four minutes exists between each spectrum which is the time-resolution in this experiment. Details can be found in the article.[27]

By changing the conventional way of controlling the instrument, acquisition of time-resolved XPS spectra with 5ms of time resolution is the main emphasis of this thesis which will be discussed later in detail in the text.

1.4. Oxide-Semiconductor Systems

Metal-Oxide-Semiconductor systems have been of particular interest to various scientific and industrial communities due to their applications in chip technology.[28,29,30,31,32]

The first uses of MOS systems date back to 1960's while 1980's and 1990's being the years during which extensive studies on characterization design and development of metal-oxide-semiconductor systems took place.[34] Ge instead of Si was used in the preliminary stages of MOS circuits. However, due to its enhanced material properties and wider applicability, Si replaced Ge almost completely later on.

Most of the MOS systems are designed to be used in computers.[33] Various MOS systems have been employed in chip industry to achieve the desired electronic properties and the smallest size possible.[34] Besides the use of silicon as semiconductor in a MOS system, other attempts to use SiGe mixtures have also been employed.

The importance of Metal/SiO_2/Si System in MOS systems lies in its stability, ease of production and promising electronic properties.[35] Unlike in the case of compound semiconductors such as GaAs or InP, Si does not decompose under certain processes during production steps. Although the mobility in Si is lower than the mobility in Ge, Si can be operated at higher temperatures without degradation and has a higher band gap than Ge. Moreover by simple thermal processes SiO_2, which is a high quality insulator, can be grown readily for many purposes including protection of underlying circuitry and patterning.

It is projected in 1999 edition of International Technology Roadmap for Semiconductors that the CMOS devices must be scaled below 100 nm in the very near future.[36] However, with today's technology it is very difficult to manufacture CMOS devices with sizes below 100 nm. The main problem is the unavailability of current top-down

lithographic techniques to produce defect-free sub-100 nm chips. Therefore the future of smaller MOS circuits and the chip industry are seen behind the realms of bottom-up approaches like self-assembly.[37]

1.5. Gold Nanoclusters

Various forms of gold nanoparticles most of which have been deposited over SiO_2 are used throughout our studies. Among these, citrate capped, TOAB (Tetraoctylammoniumbromide) capped and thiol capped ones will be ones to be described. Electrical properties, charging behavior and other structural parameters of the corresponding gold nanoclusters were studied during external biasing and TRXPS (Time resolved x-ray photoelectron spectroscopy) measurements.

1.5.1. Capped Gold Nanoparticles

Formation and preparation of capped Au nanoclusters mostly rely on the electrostatic forces that exist between the clusters and the capping agent. One of the earliest attempts to synthesize capped gold nanoparticles belongs to Turkevich et al.[38] which employed trisodiumcitrate to surround the aqueous $AuCl_4^-$ anions with citrate groups.

1.5.1.1.   Citrate-Capped Gold Nanoparticles

Upon heating these two ingredients at moderate temperatures (60^0C-80^0C), capped gold particles having a mean radius of 8 - 10 nm were prepared in Turkevich's studies.[38] These particles are characterized by UV-Vis, TEM and electrophoresis measurements. It is

shown that typically the particles exhibit a UV-vis peak at 523 nm. Upon increasing the size of the gold clusters, this peak is shown to be shifted to higher wavelengths.[39,40,41]

1.5.1.2. TOAB-Capped Gold Nanoparticles

TOAB was reported to be used as a PTA (Phase Transfer Agent) in a study by Cheng et. al.[42] recently. The transfer of Au nanoparticles from water to toluene was employed. The particles were prepared totally on the principle of electrostatic attractions between TOA^+ (Tetraoctylammonium cation) and negatively charged tannic or citrate stabilized gold nanoparticles. These charged structures were of particular importance in determination of effects of positive and negative charging as well as time constant measurements with TRXPS.

1.5.1.3. Thiol-Capped Gold Nanoparticles

Thiol capped particles were also prepared with similar procedures with other capped particles which are deposited from aqueous solution except the steps involving the incorporation of sulphur atoms to gold-bonded ends of C_{12}-alkyl chains upon addition of small amounts 1-dodecenethiol to the solution as described in the work of Brust et. al.[43] The potential changes in conductance behavior and electrical properties as well as charging of the new capped gold nanoclusters also fall in the scope of this work.

2. AIM

Previous studies[8,44] in Suzer's group have displayed the characteristics of charging under external bias in systems like Si/SiO$_2$, Al/ Al$_2$O$_3$ and W/WO$_3$ and contributed much to understanding the nature and mechanisms of charging in these systems which are of significant importance to many applications in electronic circuitry and computer industry as well as in scientific community.

However, investigation of these systems and observations of binding energy shifts and charging parameters before and after the application of external biasing could have been understood better with the possibility of monitoring the dynamics of the processes mentioned. Starting from this point, the primary objective of our studies was to find a way to disclose how the charging of a system under external bias proceeded in time. For this purpose, we have developed a novel technique and investigated the charging of a Si/SiO$_2$/Au(m) system by XPS with 5ms time resolution between two consecutive XPS spectra.

Application of the technique to other systems like gold nanoclusters deposited on SiO$_2$ and investigation of electrical and material properties of these systems were also of particular interest.

3. EXPERIMENTAL

3.1. Sample Preparation

3.1.1. SiO_2/Si System

Mostly, p-doped silicon having (100) orientation is used throughout the studies as the starting material in samples containing Si. Appropriate size of a Si substrate was cut from bigger silicon wafers and put in concentrated HF solutions for 1-2 minutes to be cleaned from already-existing oxides and other surface contaminations. Washing with distilled water and ethanol and/or acetone before drying was performed after ejection from HF solution. SiO_2 on Si substrates were grown thermally in furnace under desired temperature for variable amount of time. Thinner oxides were grown at $500\text{-}600^0C$ for 3-5 hours where thicker ones were prepared under elevated temperatures, $\sim800^0C$, and left in the furnace for several hours, i.e. ~6-12. Thicknesses of the oxide layers are determined from XPS data if the sample contains an oxide layer less than 10nm. Thicker samples are identified via Dektak measurements by etching a part of the oxide and taking the difference between the oxide layer and the Si substrate.

3.1.2. Au(foil)/SiO_2/Si System

In addition to the SiO_2/Si system mentioned above, a gold foil is attached to the rod as well. An overall scheme of the resulting setup is illustrated below in Figure 9.
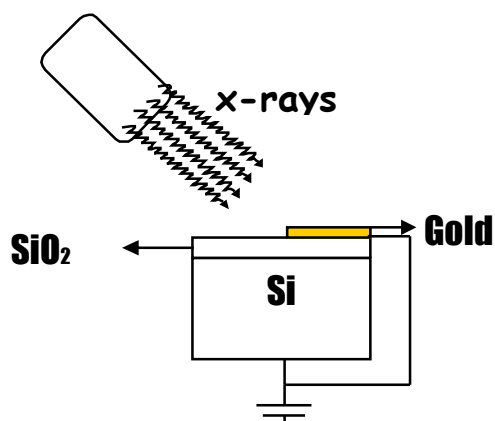
Figure 9. Au(foil)/SiO$_2$/Si System

3.1.3. Au (TOAB)/SiO$_2$/Si System

TOAB capped gold nanoparticles were prepared by the following procedure. 0.4 mL of 0.13 M TOAB (toluene) solution was mixed with 0.4 mL of the 10^{-4} g/mL aqueous gold nanoparticle solution and stirred.[42] It is observed that gold nanoparticles moved from the water layer to the toluene layer.

A few drops of TOAB solution was dripped onto the SiO$_2$/Si substrate and evaporated to form TOAB capped Au nanoparticles on SiO$_2$/Si. TOAB capped gold nanolcusters are analyzed both with and without a gold foil attached onto the Si substrate.

3.1.4. Au (thiol)/Au(foil)/SiO$_2$/Si System

Using the procedure described in reference 43, gold nanoclusters surrounded with C$_{12}$-thiol groups are prepared.[43] In addition to the nanoclusters deposited on SiO$_2$ by evaporation decribed above, Au foil is also attached to the rod for mainly referencing purposes. The resulting setup is depicted in Figure 10.
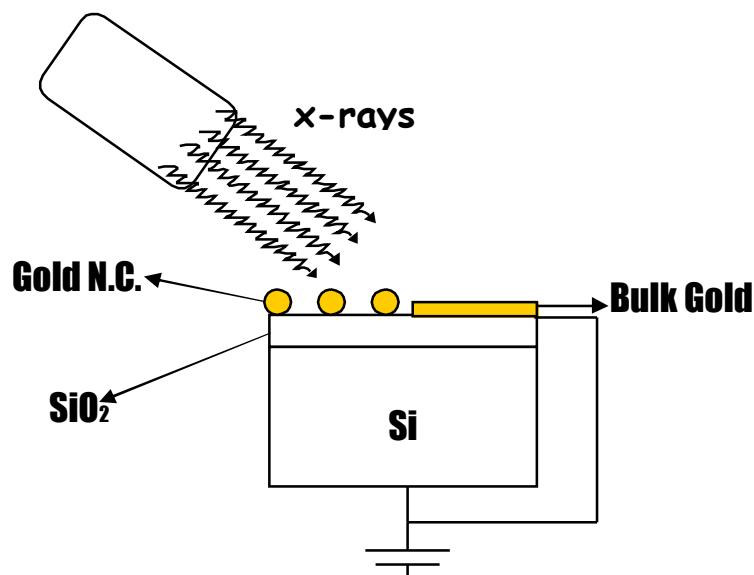
Figure 10. Au (thiol)/Au(foil)/SiO$_2$/Si System

3.2. Instruments and Techniques

3.2.1. XPS

All of the XPS spectra were taken with a KRATOS ES300 X-ray Photoelectron Spectrometer with a non-monochromatized MgK$_\alpha$ source (1253.6 eV). Pressure of the analysis chamber was kept around 10^{-9}-10^{-8} Torr. For peak fitting in still and time-resolved measurements, XPSPeak95 v2.0 is employed.

3.2.2. Hardware

Two AD/DA cards (ADA2110 of Real Time Devices Inc. and Super 16-Bit AD/DA of Industrial I/O Cards) are used in data acquisition along with an integrated timer card. One of the AD (28 µs) / DA (2 µs)'s was a 16-bit DAQ card with eight analog inputs and 2 analog outputs. The other AD (20 µs) / DA (10 µs) used had 12-bit analog output resolution with a

16-bit timer card having an 8MHz internal oscillator. A Pentium-II is used to administer the data acquisition.

3.2.3. Software

Time resolved XPS measurements were recorded with home-made software which was coded in Visual Basic in our labs. Other XPS spectra were taken by a program designed for conventional XPS analysis.

3.2.3.1. Visual Basic

Except for the module which governs 'read/write' operations directly by taking advantage of a dynamic link library code, no special modules/sub-modules/macros or predefined codes were used. The entire program was coded in Visual Basic 5.0.

3.2.3.2. The Program

The program uses two analog output channels, one analog input, built-in analog-to-digital digital-to-analog converters and three programmable timer-counters simultaneously to control the spectrometer during data acquisition and has a simple yet friendly graphical user interface (GUI). The GUI of the program is shown below in Figure 11.
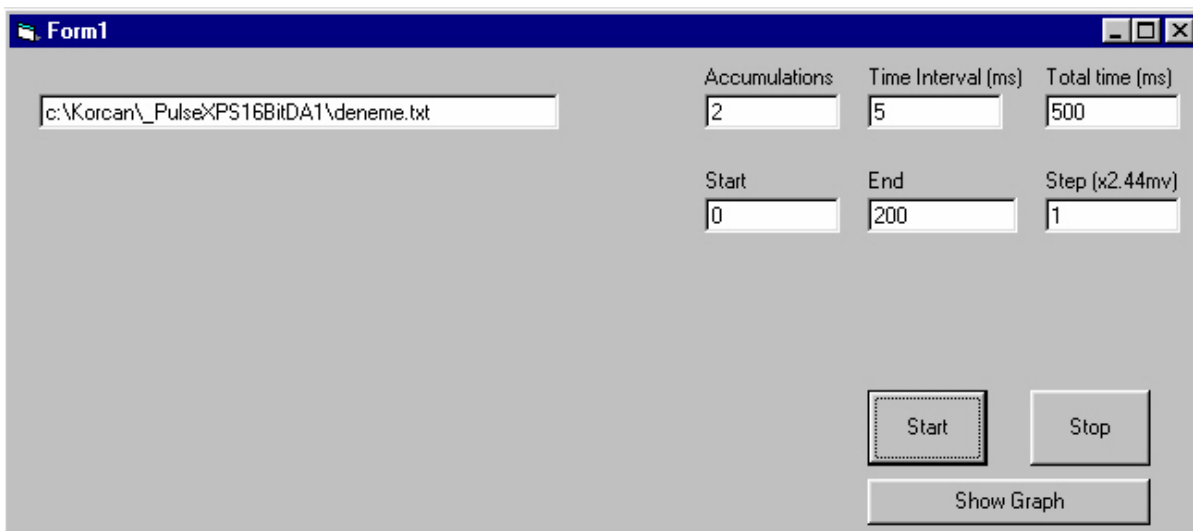
Figure 11. A screenshot of the GUI of the program coded in Visual Basic for time resolved

XPS measurements.

As it is also seen in the screenshot of the program above, the program accepts several parameters from the user. In the upper row, under 'accumulations' tag, the number of cycles that the program will perform the monitoring process is entered. Next to 'accumulations' tag, the desired time resolution between two consequent spectra is requested from the user. The data field on the right in the upper row is the total time during which the charging process is being monitored. The first two fields in the second row are the start and end points which specify the energy frame for the measurement where the field on the right is the energy resolution.

3.2.3.2.1. The Logic

The logic simply lies behind the following idea. Instead of imposing a bias on the sample and shifting the whole energy frame to see the desired peak in its new position

23

afterwards, individual binding energy values that belong to the desired energy frame in which the peak will appear after the application of the bias is monitored immediately after the application of the bias. The process is repeated until all the energy steps that fall into the frame to be monitored are completed.

3.2.3.2.2. The Code

The incorporation of the above logic to a computer code is relatively simple for an intermediate programmer. One of the analog outputs governs the sample voltage while the other is responsible for the energy axis. The code orders the spectrometer to 'sit' at a specified binding energy value and tracks the changes in the intensity while the sample voltage is repeatedly altered between two selected bias voltages. Each of the intensity changes are recorded in the meantime with appropriate energy information and stored in a data array to speed up the functioning of the program. The array is then written to a file at the end of the data acquisition.

3.2.3.2.3. Pulse Counting

Electron pulses are counted with integrated programmable timer-counter card. One of the 16-bit timer-counters was referenced to the internal 8MHz oscillator and employed to keep the real time in milliseconds. The second one was used particularly for time keeping in a stopwatch manner to govern the individual pulse counting periods. The last one, working in sync with the second one, was used in the detection of the pulses.

3.3. Application of Time Resolved XPS (TRXPS)
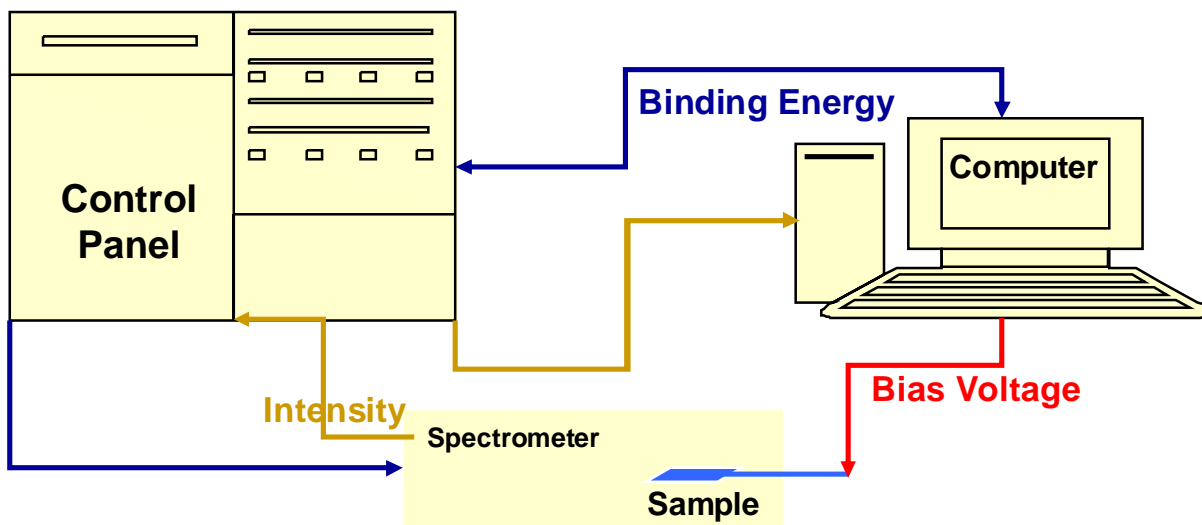
Figure 12. The setup used in TRXPS measurements

As displayed above in Figure 12, application of the computer controlled bias voltage required one more connection from the computer to the sample in addition to conventional connections that are required to obtain a normal XPS spectrum.

3.4. External Biasing

All bias voltages were simply applied to the sample rod which carried the sample by corresponding power supplies. Si was directly in touch with the voltage supply through the rod during still measurements. In the cases when a gold foil is used, the foil was also contacted with the rod as in the case of Si. Analog output of the AD/DA card was connected to the sample rod in the case of TRXPS measurements.

3.4.1. External Resistance

Various ohmic resistances ranging from a few ohms to a few hundredths of mega-ohms were used throughout the studies all of which were connected in series to the sample rod.

3.4.2. External Capacitance

Since connecting a capacitor in series without another element to the sample means nothing but an open circuit, the capacitors were connected in parallel with other circuit elements, particularly resistors. Capacitance values of the capacitors were changing from pico farads to micro farads depending on the desired RC values.

3.4.3. RC Measurements

Resistances and capacitors which are connected in parallel with each other but in series with the sample are used for RC measurements.

3.5. Electron Flood Gun

The gun is composed of a tungsten filament which emits electrons inside the vacuum upon passing a current through its ends. The current was controlled with a variable current-voltage power supply. The filament current was varied between 3-3.6A throughout the measurements. When needed, the filament was floated with a few (-) volts ranging from 0 to -6Volts with another D.C. power supply. The overall picture illustrating the setup for supplying extra low energy electrons to the system is shown in Figure 13.
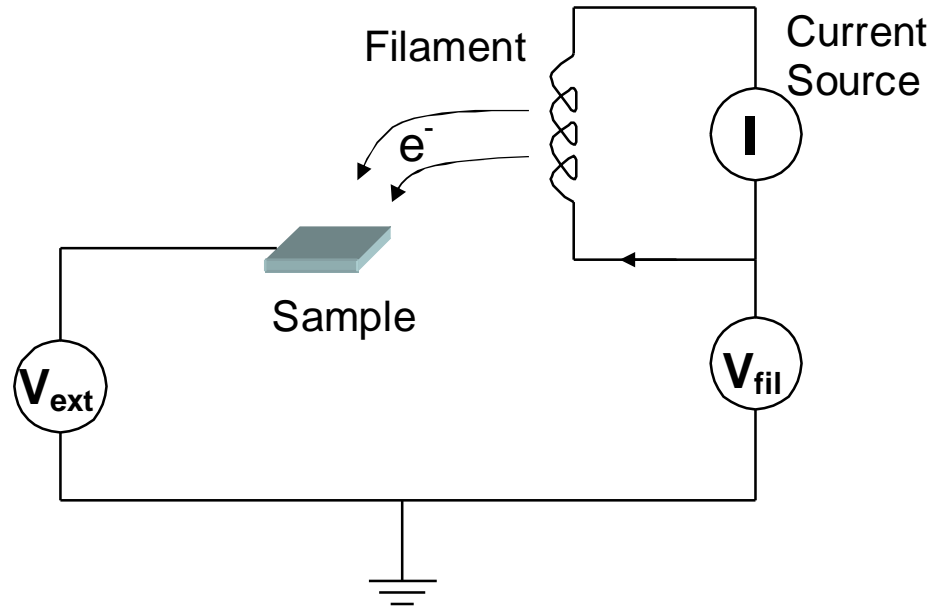
Figure 13. Equivalent circuit of the system used for application of low energy electrons inside the vacuum chamber.

4. RESULTS AND DISCUSSION

4.1. External Biasing Measurements with Si/SiO$_2$ System

As explained earlier in the introduction part, upon application of a fixed magnitude of positive and negative bias to Si/SiO$_2$ system, corresponding shifts induced in oxide Si2p photoemission towards higher and lower binding energies are not the same in magnitude. Thus, one observes a lesser shift to a higher binding energy under negative charging, i.e. positive biasing, where again a lesser shift to lower binding energies in the case of positive charging, i.e. negative biasing, is observed. This asymmetric behavior is attributed to the differences in the mechanisms of positive and negative charging.[8]

The value of this differential shift was found to be dependent on the magnitude of the bias and it was shown that it saturates after 10V.[8] Therefore, to cover the range that responds most to the applied biasing in terms of observed shifts in binding energies, the experiments were mostly carried out within ±10V.

As also displayed in Figure 9, gold was connected on top of Si/SiO$_2$ layer for referencing purposes. Being a perfect conductor, gold, as in many other previous XPS studies, was introduced to determine the amount of charging in SiO$_2$ layer under external bias accurately. It is observed that gold indeed displays exactly the same amount of shifts as the applied external bias within the detection limit of our instrument which is ±0.1eV.
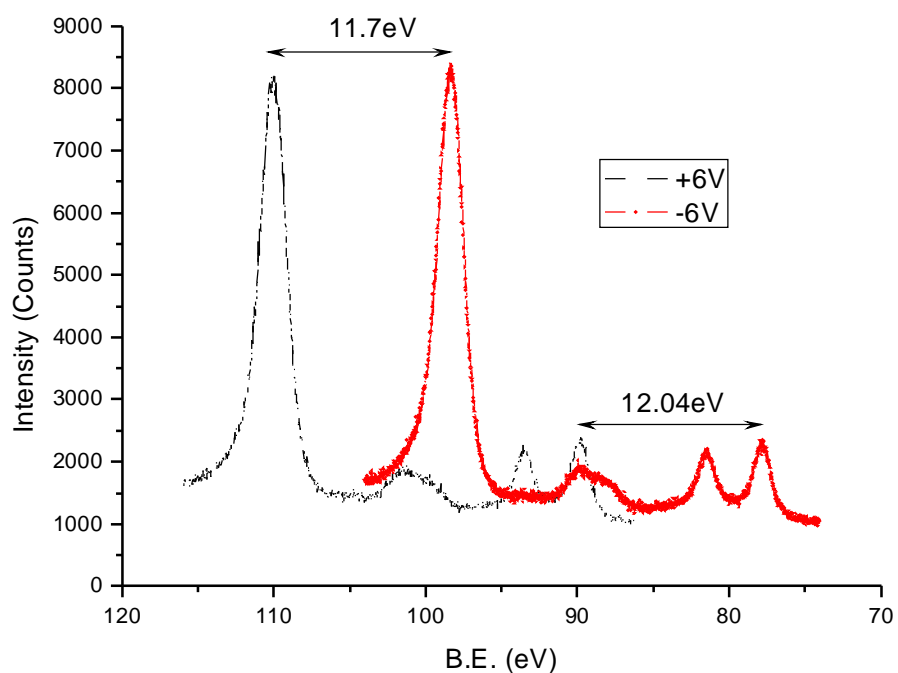
Figure 14. Relative differences in energy changes of Gold, which was used as a reference, and SiO_2, under +6V and -6V.

Figure 14 implies that Au 4f peaks exhibit a shift of 12.04eV which is almost exactly the total amplitude of the biasing. However, the difference between two Si2p peaks is about 11.7eV. This 0.34eV difference is significant and well above the detection limit providing the driving force for carrying out external bias and differential charging measurements.

Instead of taking the difference between two Si2p peaks in two different cases of external biasing, the difference of Si2p with respect to reference, i.e. gold, is taken throughout our studies to track the changes in charging of SiO_2.

Voltage	Si 2p B.E. (eV)	Si 2p FWHM (eV)	Au 4f B.E. (eV)	Si2p-Au4f
+6V	109.88eV	1.69eV	89.84eV	20.04eV
-6V	98.18eV	1.64eV	77.8eV	20.38eV

Table 2. Tabulated values of binding energies of silicon and gold upon application of +6V and -6V

The binding energies of gold and silicon at -6V and +6V and FWHM values of silicon at these two voltages are shown in Table 2. The full width of Si2p peak at its half maximum (FWHM) does not change much in this case.
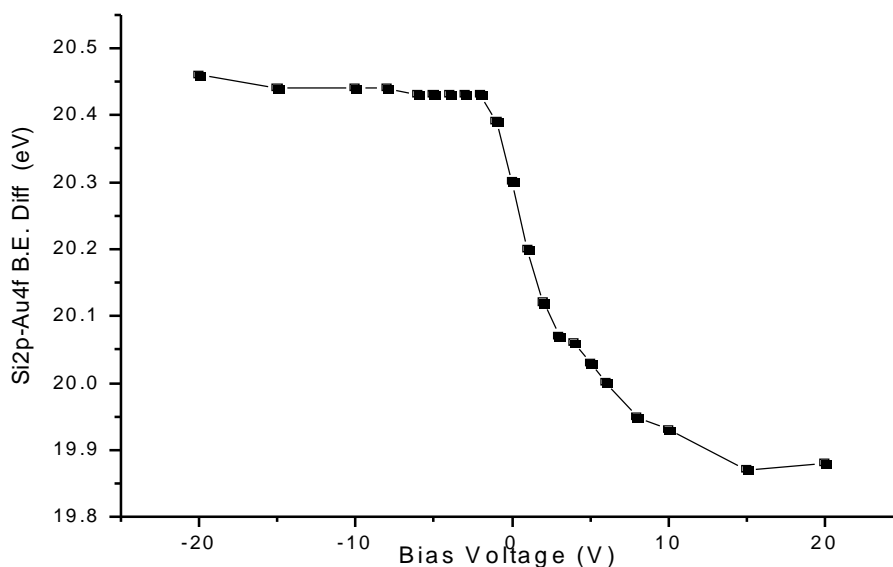
Figure 15. The change in binding energy of Silicon with respect to Gold as a function of

external bias.

Si2p-Au4f binding energy difference is plotted versus external bias in Figure 15. The oxide in this sample was grown at 600^0C for 3-4 hours and the thickness of the oxide is estimated to be around 10 nanometers. Voltage dependence of the observed shifts is clearly seen in the above figure that as the magnitude of the voltage increases, the binding energy difference between Si2p and Au4f deviates either above or below from its reference value, i.e. the value found upon grounding the system. The positive voltage simply alters the amount of electrons attracted to the sample and thereby controls the negative charging process on the surface. Conversely, a negative voltage again alters the amount of electrons that help surface neutralize, but in the opposite way.

One can easily recognize the immediate saturation around -2 Volts while going towards increased negative bias. This behavior is attributed to the easiness of repelling low energy stray electrons even at low negative voltages such as -2-3V. In the case of positive biasing however, the difference saturates at a considerably higher voltage value, around 15V meaning that nearly all of the stray electrons that could help the sample charge negatively are attracted to the surface and the sample can not be neutralized further more by means of an increased positive potential.

4.1.1. The Effect of Low Energy Electron Bombardment

In the case of negative charging, it was also shown in Table 2 that the difference between Si2p and Au 4f decreases. As also mentioned in the work of Ülgüt and Süzer[8], stray electrons that are attracted towards the sample surface are shown to be the primary cause of this neutralization. The filament acts as an additional low energy electron gun. The current passing through the filament of the electron gun and the energies of the emitted electrons determined by floating the filament are varied to study the effects on the corresponding shifts.

Voltage	Si 2p B.E. (eV)	Si 2p FWHM (eV)	Au 4f B.E. (eV)	Si2p-Au4f
+6V-As is	109.88eV	1.69eV	89.84eV	20.04eV
+6V-3.4A	108.89eV	1.91eV	89.82eV	19.07eV
+6V-3.6A	108.59eV	2.05eV	89.81eV	18.78eV
-6V-As is	98.18eV	1.64eV	77.8eV	20.38eV
-6V-3.4A	98.2eV	1.73eV	77.81eV	20.39eV
-6V-3.6A	98.18eV	1.78eV	77.8eV	20.38eV

Table 3. Results of different filament currents on the binding energy values and FWHM of

silicon oxide grown at 800^0C for 7h and bulk gold.

In Table 3, the changes induced in the system upon introduction of low energy electron emission are tabulated. The first thing to note here is the decrease in the binding energy of the silicon 2p photoemission with increasing filament current such that a downward shift of approximately 1.2eV is created as the filament current increases to 3.6 Amperes. Gold on the other side does not exhibit any significant changes. Therefore, the difference in the binding energies of silicon and gold decreases from 20.04eV to 18.78eV, pointing out an increase in the amount of negative charging. The FWHM values of Si2p also change accordingly from 1.69eV to 2.05eV indicating that the medium from which the Si2p photoemission signals are collected has become more inhomogeneous in terms of local potentials. On the other hand, filament emission does not seem to change much of the charging picture in terms of peak positions in the case of positive charging, i.e. under

negative bias. Going from no filament emission to 3.6A emission current, the FWHM of Si2p photoemission decreases to 1.64eV from 1.78eV.

These findings on positive and negative charging have led our studies to use external biasing together with low energy electron emission for extraction of useful information from the sample.

4.2. External Bias Induced Separation of Au-4f Peaks in Si/SiO$_2$/Au(Cluster)/Au (foil) System

External bias measurements can be used in harvesting valuable chemical information. For this purpose, TOAB capped gold nanoclusters were prepared using Brust's method[43]. A few drops of this solution containing the clusters were dripped onto a Si/SiO$_2$ substrate and the solution was evaporated for the gold nanoparticles to be deposited over the oxide layer, which was approximately 20 nm thick. Low energy electron emission was also turned on for additional neutralization and enhanced peak separation. As described earlier in the introduction part, a gold foil is also attached to the Si/SiO$_2$ substrate. The scheme was illustrated in Figure 10 on page 20.

As depicted in Figure 16 b), gold 4f peaks that belong to nanoclusters and the bulk gold are overlapped when the sample is grounded. This is in the case of zero or negligible charging. However, upon application of positive and negative biases, two different Au 4f peaks coming from two different environments are separated by a well defined energy. Figure 16 a) and c) show this separation clearly. One also notes that the absolute amounts of separation observed in positively and negatively charged cases are not identical.
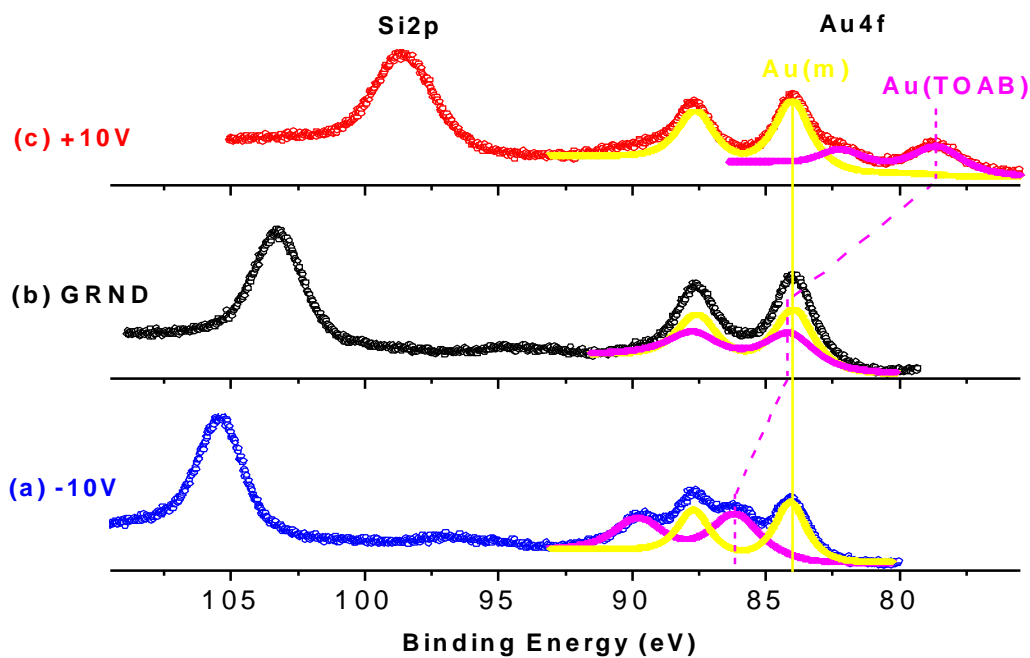
Figure 16. External bias induced separation of Au 4f peaks in a substrate containing gold both as nanoclusters capped by TOAB and in its bulk state.

The difference in the behavior of gold nanoclusters is mostly due to the fact that nanoclusters follow closely the potential created in the oxide layer. In the case of negative bias, oxide peak lags behind and does not exhibit a-full-10V-shift towards lower binding energies since the repellence of stray electrons from the surface causes the oxide layer to be less negative. Being deposited on top of the oxide layer and following the same charging route, gold nanoclusters, display a similar if not identical charging behavior. Similarly, the change in the peak position of Si2p photoemission in the case of +10V with respect to its grounded value is approximately the same as the difference between two Au 4f signals under +10V indicating that upon attraction of a greater number of low energy electrons to the

sample, the neutralization takes place more efficiently causing the silicon oxide peak, together with the 4f peak of the nanoclusters to shift less towards higher binding energies.
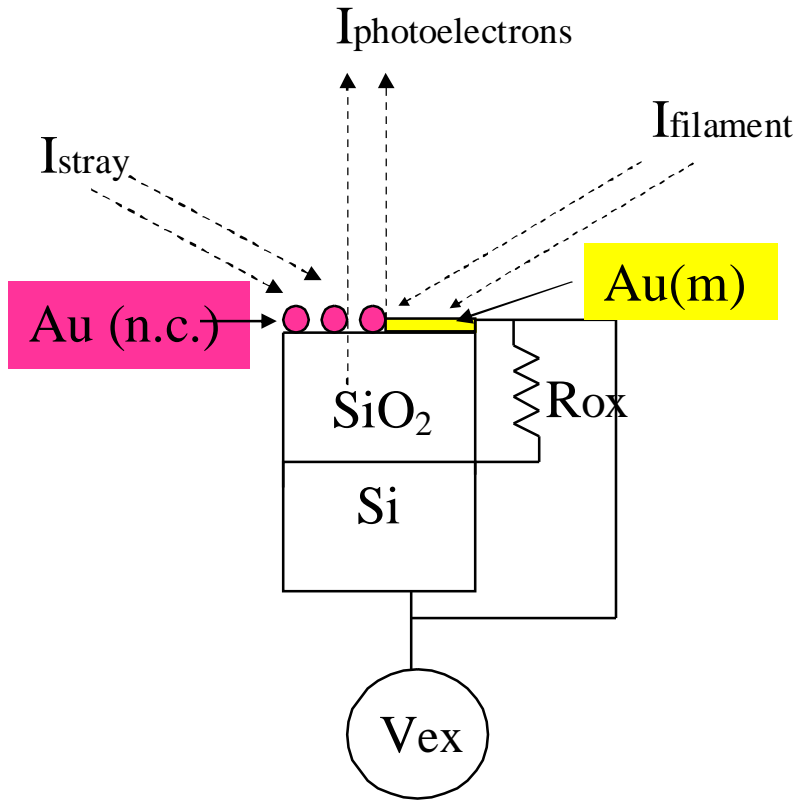
Figure 17. An electrical model of the system described above.

The electrical connections and a model of the system showing the different forms of gold and the oxide layer are given in Figure 17.

4.3. TRXPS Results of Various Systems

The time-resolved technique has first been applied to Si/SiO_2 system since the behavior of this system under external bias was extensively studied by our group before. Together with characterization of time dependent behavior of Si/SiO_2, other systems like

Si/SiO$_2$/Au (foil) and Si/SiO$_2$/Au (TOAB nanoclusters) are also studied with time resolved X-ray photoelectron spectroscopy.
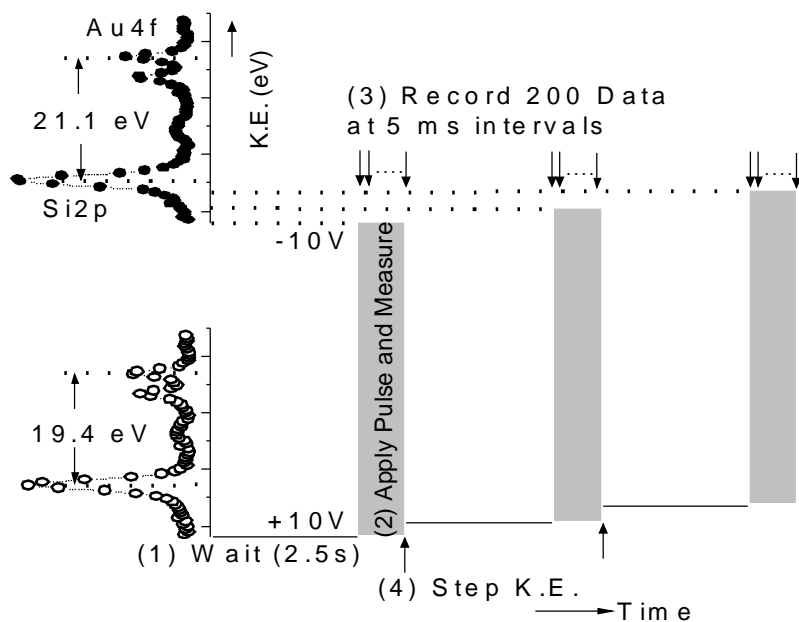
Figure 18. An illustration of the time resolved XPS data acquisition process

A typical data acquisition process is shown above. The voltage pulse is +10V to -10V in this case with a delay period of 2.5s. First, the sample is kept at +10V for 2.5s and the response of the system immediately after switching the bias voltage to -10V is then recorded with 5 ms intervals. The same procedure is repeated for each energy points to collect a full spectrum. The data acquisition procedure is also reversible such that the sample can be hold at -10V for a desired amount of time and the time dependent data can be collected upon switching the voltage to +10V yielding the reverse of charging/discharging process.

4.3.1. Si/SiO$_2$ System

As it has been described before, a gold foil is attached to serve as a reference on top of a SiO$_2$ layer throughout the TRXPS measurements when the oxide layer is thick enough to mask the photoemission of bulk silicon substrate. In cases where Si^0 peak of the substrate is also observable, Si^0 photoemission is monitored together with Si^{4+} in the spectra.

An example of such a spectrum where both of the silicon peaks coming from the substrate and the oxide overlayer are shown in Figure 19.
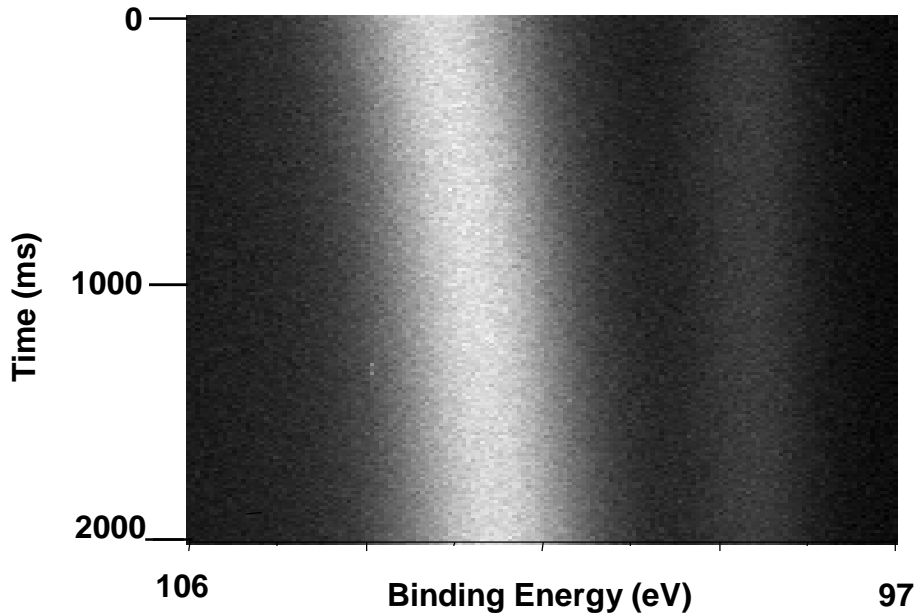
Figure 19. TRXPS spectrum of a Si/SiO$_2$ system showing the silicon region. The changes in Si^0 (right) and Si^{4+} (left) peaks in time are shown together.

The oxide here is 6 nm thick. The spectra is recorded at -10V immediately after changing the external bias voltage from +10V to -10V. Two hundred XPS spectra of silicon region with a time resolution of 5ms are collected in 1 second after the application of -10V. The figure above is a top-view of the collection of the resulting spectra displaying the time

evolution of peaks. By tracking the changes in peak maxima, investigation of the response of the system to the change in external bias is obtained.

It is shown that despite the changes in the position of the silicon peak of the oxide in time, no signs of time dependent changes are observed in the position of the signal coming from the underlying silicon substrate.

4.3.2. Si/SiO$_2$/Au(nanocluster) System

This system was different than the thin Si/SiO$_2$ system from two aspects; first, the oxide was considerably thicker compared to the previous situation of ~6 nm, which was estimated to be 400 nm thick preventing observation of the Si^0 peak. Secondly, gold in its metallic form as foil was introduced to the system. The energy range was selected such that the gold and the oxide silicon are displayed together in the spectra for comparison and referencing purposes. The TRXPS results of this system showed the clear-cut time dependent charging behavior of the thick silicon oxide layer.[45]

One of the first results immediately noted is that gold does not exhibit a time dependent charging shift whereas silicon completely undergoes a time dependent exponential charging shift in the same period. The binding energy difference measured between Si2p and gold under +10V was 19.4eV. In the negative biasing case, this difference rises to 19.4eV+ΔV.

Assuming that the oxide layer has a finite resistance and capacitance, this exponential shift that is displayed by the oxide layer is analyzed, and by fitting the peak maxima, an approximate time constant for charging of the oxide layer is obtained as shown in Figure 20.
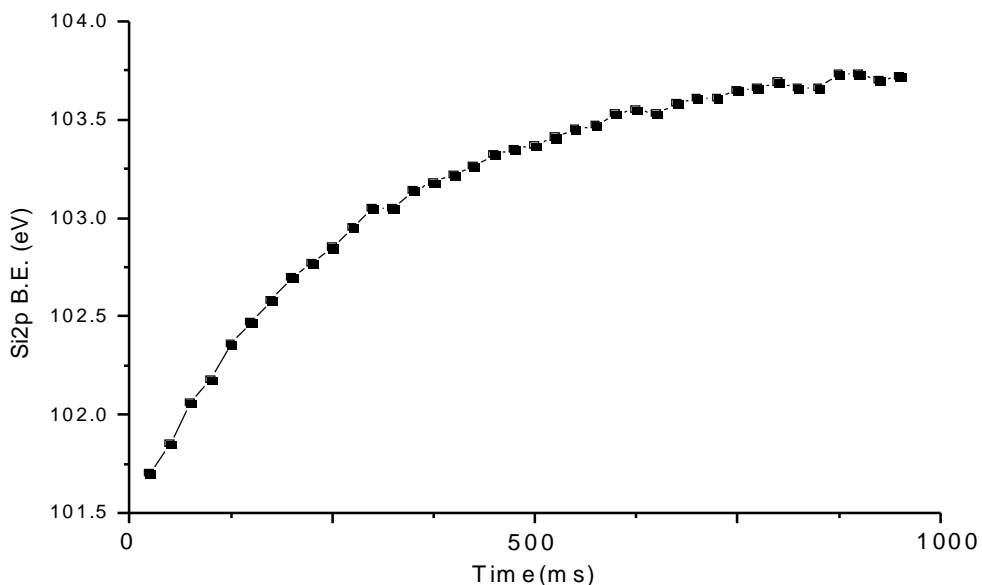
Figure 20. The peak maxima of oxide Si2p photoemission versus time.

A total breadth about 2eV in the charging amplitude is observed with an error range of ±0.1eV. A first order exponential fit of the derived binding energy values gave an RC value of ~300ms which is consistent with previous values derived from time dependent leakage currents and other techniques such as scanning capacitance microscopy.[46,47,48,49] Since the photoemission and related processes are happening at much smaller time-scales (picoseconds), this charging curve is attributed to the trapping/detrapping of the holes in the valence band of the oxide layer.[45,28] Since this time constant is a measure of the product of the resistance and the capacitance of the oxide layer, one needs to determine either an approximate value of the resistance or the capacitance of the oxide from another reliable technique.

In addition to the oxide layer grown on the silicon substrate, thiol-capped gold nanoclusters were also deposited on top of the oxide overlayer to investigate the electrical properties and responses of the resulting surface nanostructures.
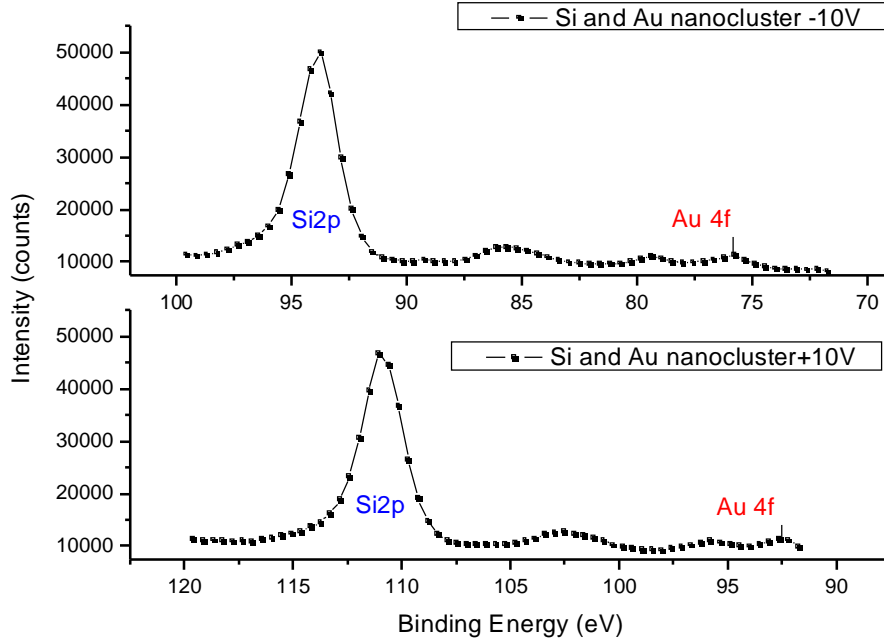
Figure 21. XPS spectra showing Si2p and Au4f regions taken under +10V and -10V.

The response of the system under positive (+10V) and negative (-10V) bias is shown in Figure 21. The positions of the peak maxima are shown just above the corresponding peaks. Upon taking the differences of the line positions indicated as reds and blues in both spectra, it is found that the separation of gold and silicon oxide peaks increases upon application of positive external bias when compared to the decrease observed in the case of negative biasing.
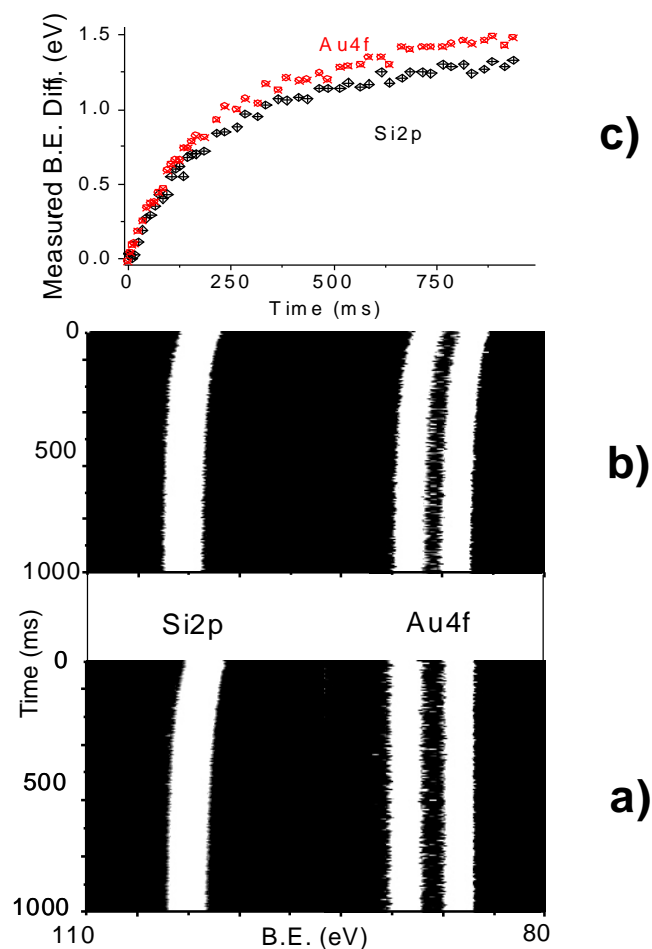
Figure 22. Time-resolved XPS spectra of the Si2p-Au4f region of (a) a Si/SiO$_2$ sample containing a ca. 400-nm oxide layer and a gold metal strip connected to it and (b) the same sample onto which C$_{12}$-thiol-capped gold nanoclusters are deposited. Charging curves of the two components that are obtained by curve fitting of the individual time resolved XPS data are shown in (c).

Figure 22 a) shows the response of the system to the pulsing sequence. The system was waited at +10V and then pulsed to -10V for the time resolved spectra to be recorded with a time resolution of 5ms. The results showed that gold nanoclusters deposited on silicon

displayed a very similar charging behavior under external bias as the oxide layer. Unlike the situation in its bulk form as shown in Figure 22 a), Au 4f photoemission coming from gold nanoparticles displays an exponential shift over time which is clearly seen in Figure 22 b). The shifts in peak maxima of Si2p of the oxide and Au4f of gold nanoclusters are also plotted on top of each other in Figure 22 c). Despite the similarities mentioned above, a slight but not-to-be-underestimated difference exists in the course of charging curves of gold and the oxide.
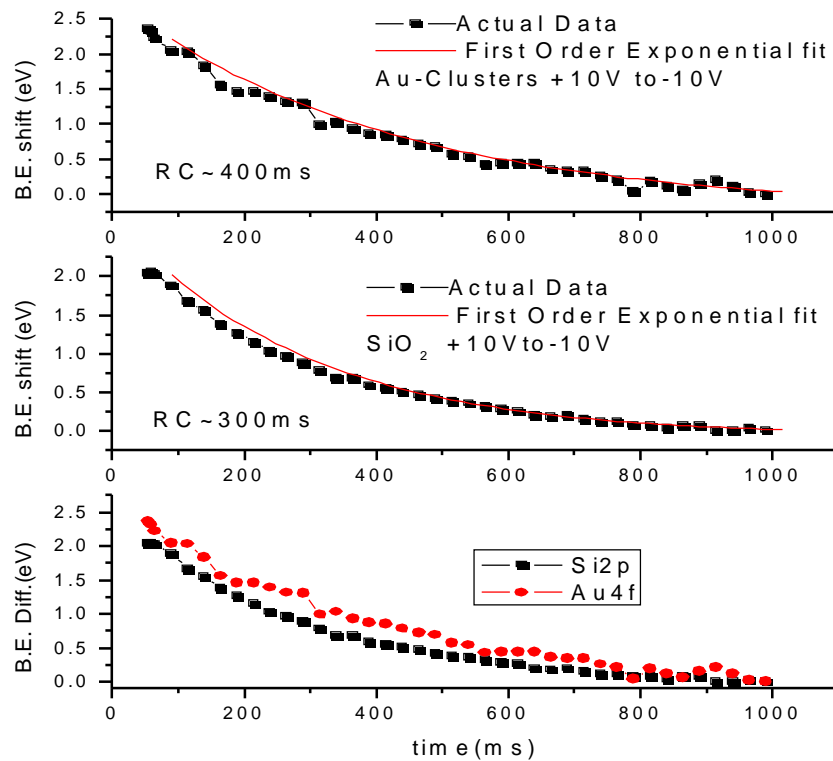
Figure 23. Exponential fits of the charging curves for Si2p and Au4f. The shifts are transformed into decay curves for better fit analysis.

Figure 23 shows more in detail the slight but detectable differences in the time dependent shifts of gold and silicon under external bias. The two curves for Si2p and Au4f

43

end up almost with the same point in the bottom graph in Figure 23, although their starting points in the energy scale are different. Moreover, there also exists a difference in RC time constants of the silicon oxide and the gold clusters as shown in the insets of Figure 23, yielding 300ms and 400ms for the oxide and gold nanoclusters, respectively. This indicates that the gold nanoclusters react slower than the oxide layer under identical conditions. This is also confirmed by inspection of Figure 22. While shifting towards higher binding energies under positive bias, silicon oxide shifts more than the clusters. Similarly, gold falls behind the oxide layer in terms of shifts towards lower binding energies and cannot shift as much as silicon upon application of a negative bias, resulting in a decrease in the difference between the two.

4.4. Effect of Low Energy Electron Gun on Binding Energy Shifts and Time Constants
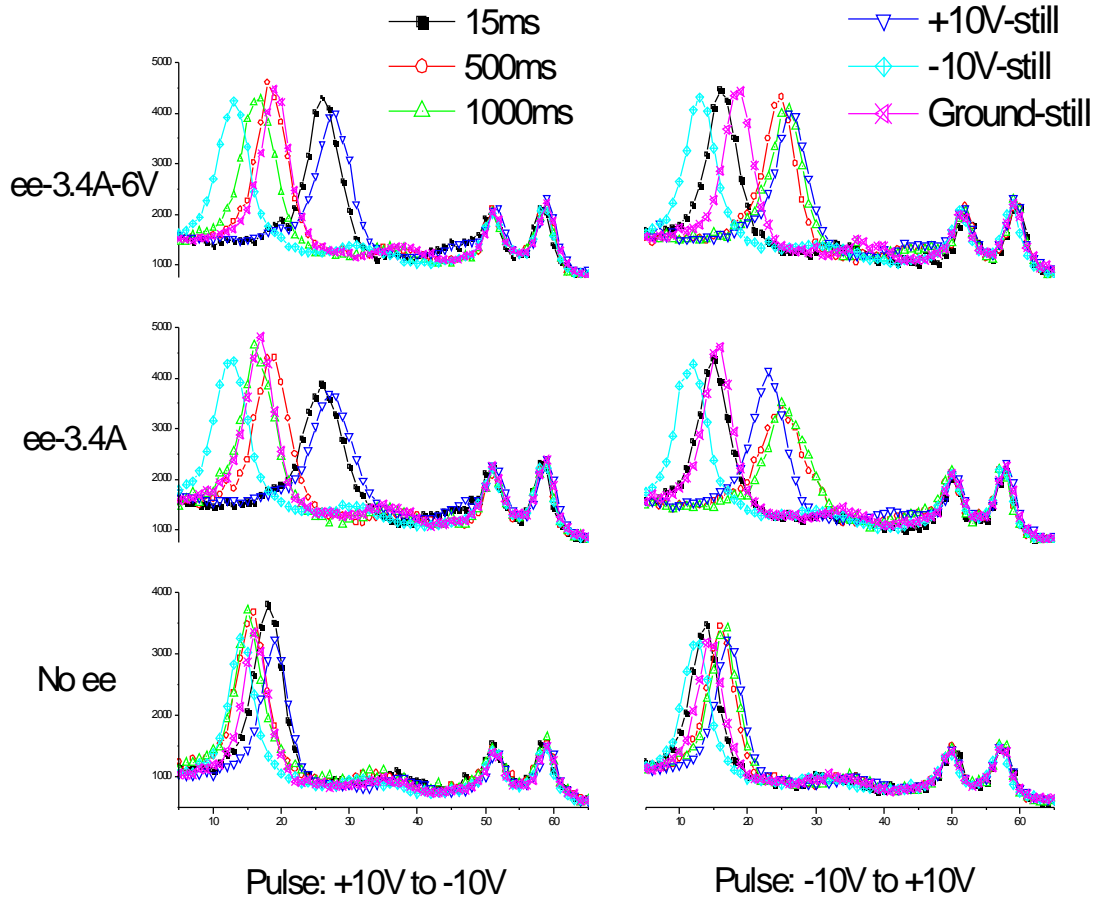
Figure 24.. XPS spectra demonstrating the effect of low energy electron emission on the binding energies and the time dependent behavior. Rows show spectra taken at different electron emission levels whereas two different pulses are illustrated in two columns. In each of the six graphs, spectra taken under +10V, -10V bias and grounded cases with time resolved spectra at 15ms, 500ms, and 1000ms after the application of the external bias are shown.

Our studies on the effect of low energy electron emission on systems under external bias are summarized in Figure 24. Going from no electron emission to 3.4A filament current, the absolute binding energy shifts observed upon application of positive and negative bias are amplified irrespective of the direction of the pulsing step. Although some changes are noticed upon detailed inspection of the corresponding spectra, floating the filament with -6V does not seem to change much of the situation compared to the case of zero floating. Therefore, in general it is observed that the low energy electron emission helps neutralize the surface and magnifies the binding energy shifts observed under external bias.

4.5. Dependence of Time Constant on Photoemission Current

To study the effects of photoemission current on the charging/discharging time constants, the emission current is varied during the analysis of a thick oxide that has an oxide layer of approximately 400 nm thick. The exponential effect of increasing the photoemission current is clearly seen in Figure 25. The time constants observed in a 400nm-thick oxide layer decrease with a non linear behavior from 280ms to 100 ms as the emission current rises from 2mA to 12mA. This non-linear dependence of time constants on photoemission current strongly suggests that the photoemission process is actively involved in the charging/discharging mechanisms that are being investigated. However, it must be noted that the time constant saturates after 12mA photoemission current meaning that filling of holes created during the photoemission process by the stray electrons has a limit.
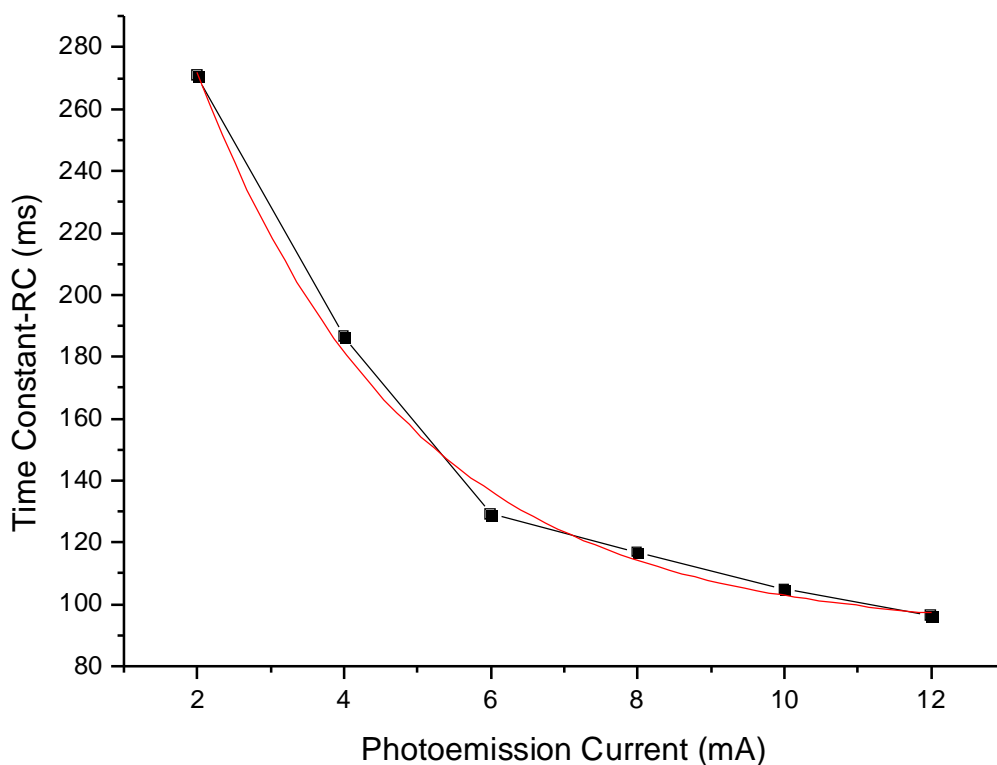
Figure 25. The effect of increasing the emission current on the time constants. The step

voltage is -10V to +10V. A first order exponential decay fit is shown in red.

4.6. Variation of Delay Period

As described earlier in this thesis, while taking time resolved spectra, the system is kept at a specified external bias for a finite delay period before the application of the target pulse voltage and acquisition of the time dependent data. To understand the function of the delay period, a series of measurements with same pulses and sample conditions are made at various delays.

~8nm-SiO$_2$ Pulse: -6Vto+6V   EE: 3.6A-2V
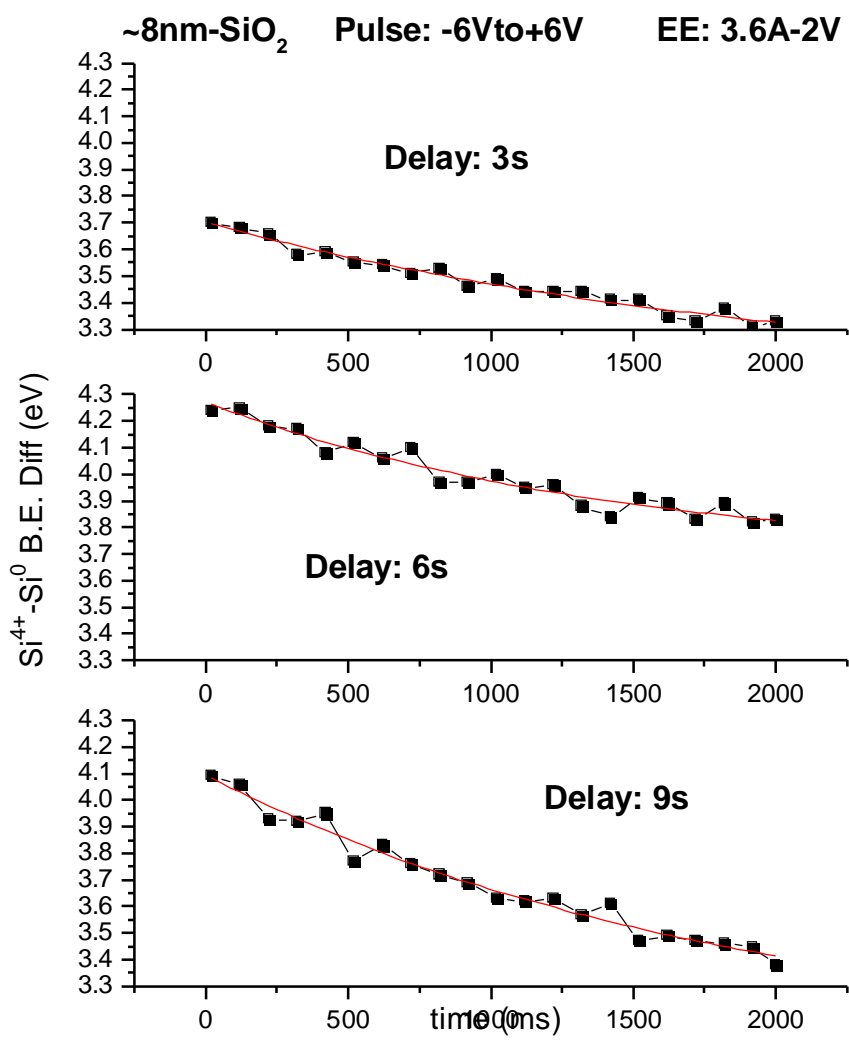
Figure 26. Si2p(oxide)-Si2p(Si substrate) differences are plotted versus time for measurements performed on the same sample which was approximately 8 nm thick. The pulse was from -6V to +6V and the electron emission (ee) was turned on during the experiments. Delay period is varied between 3s and 9s with 3s increments.

It is seen in Figure 26 that changing the delay does not cause dramatic changes in the time constants of the system such that the silicon oxide layer is found to be charging with an

RC constant of 2 seconds in all three cases. Another thing that is noted in Figure 26 but more clearly seen in Figure 27 is that as the delay period is increased, the overall charging amplitude is increased. The difference in the amplitude of charging is within experimental error limits although one can notice a slight change when going from 3s to 6s data. On the other hand, the rise in the amplitude is much clearer, totaling to a value more than 0.4eV, in the experiment in which the sample is hold for 9s at the settle voltage. It can be inferred from the data that the system needs time to equilibrate and responds fully to the pulse voltage as the electrical parameters get closer to equilibrium. As an optimum value, a delay period of 6s is commonly used in most of the measurements unless another value is stated.
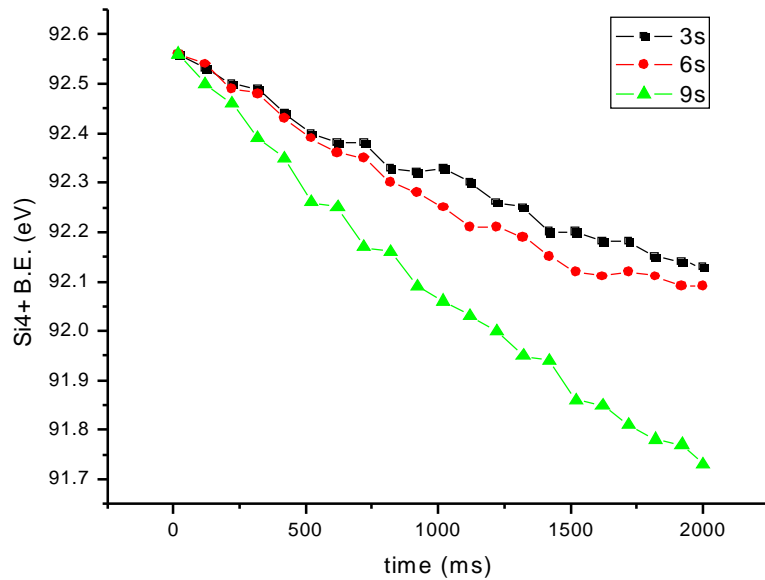
Figure 27. Decay of silicon oxide Si2p peak with time in measurements having different delay periods. The starting points of the curves are superimposed on each other for a better view of the delay-dependent changes.

Aside from the changes in binding energies, the FWHM values of the Si2p-oxide peak do not exhibit a significant change during the time dependent charging shift. Moreover, the FWHM values of the data recorded under different delay periods are almost the same in all three measurements.
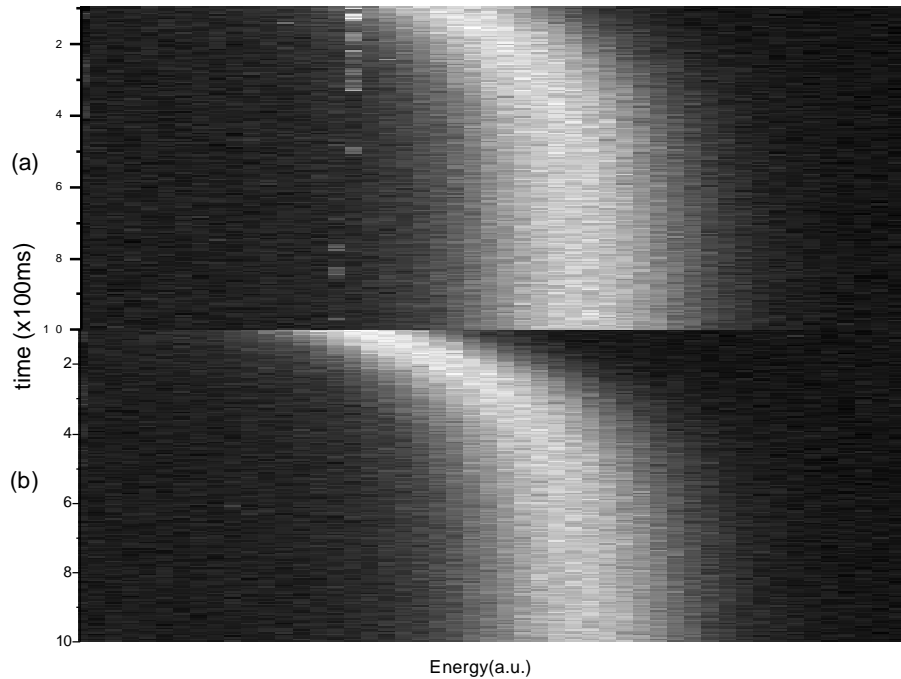
Figure 28. TRXPS results of silicon region of a sample with varied delay periods (a) 1s and (b) 6 s. The sample was approximately 40 nm thick and the step was -10V to +10V.

In another sample, which was thicker (~40 nm) than the previous sample the same effects are observed upon changing the delay period. Figure 28 shows two time resolved spectra taken at 1s and 6s delays. Since the sample is thick enough, Si2p photoemission of the underlying Si substrate is not observable and only the silicon oxide peak is shown. In going from (a) to (b), it is seen that the starting point of the charging shifts, indicating that

50

initially the sample was more negatively charged when it is kept at -10V for 6 seconds than the situation is was under -10V for 1 second. This result is totally consistent with the previous discussions.

4.7. Effect of Sample Thickness on Time Constants

To demonstrate the dependence of time constants on sample thickness, two samples having app. 4 nm and 30 nm oxide thicknesses are analyzed under the same experimental conditions.
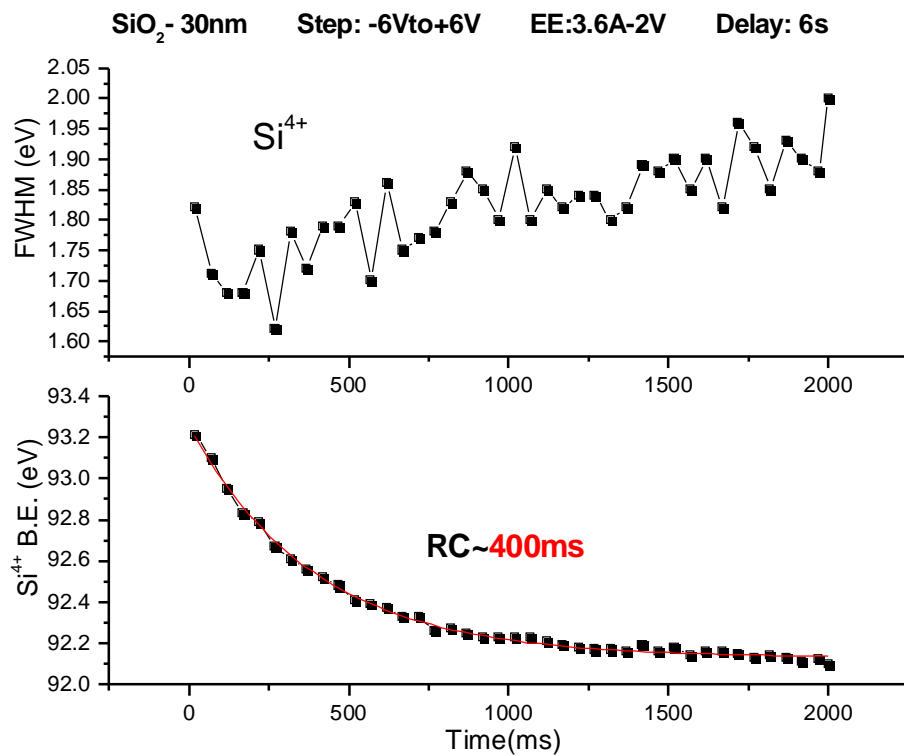
Figure 29. FWHM and the Si2p peak position of silicon oxide which is approximately 30 nm thick.

In the figure above, the charging behavior of a 30-nm-thick sample is depicted upon application of a -6V to +6V voltage pulse. The electron emission was turned on to amplify the observed shifts and the filament was floated with -2V. A first order exponential decay fit of the Si^{4+} peak maxima gives the time constant of the 30-nm-thick oxide layer as 400ms, which is a value that is in harmony with the previous measurements. Meanwhile, the FWHM of the oxide peak also shows a slight but detectable time dependent increase.
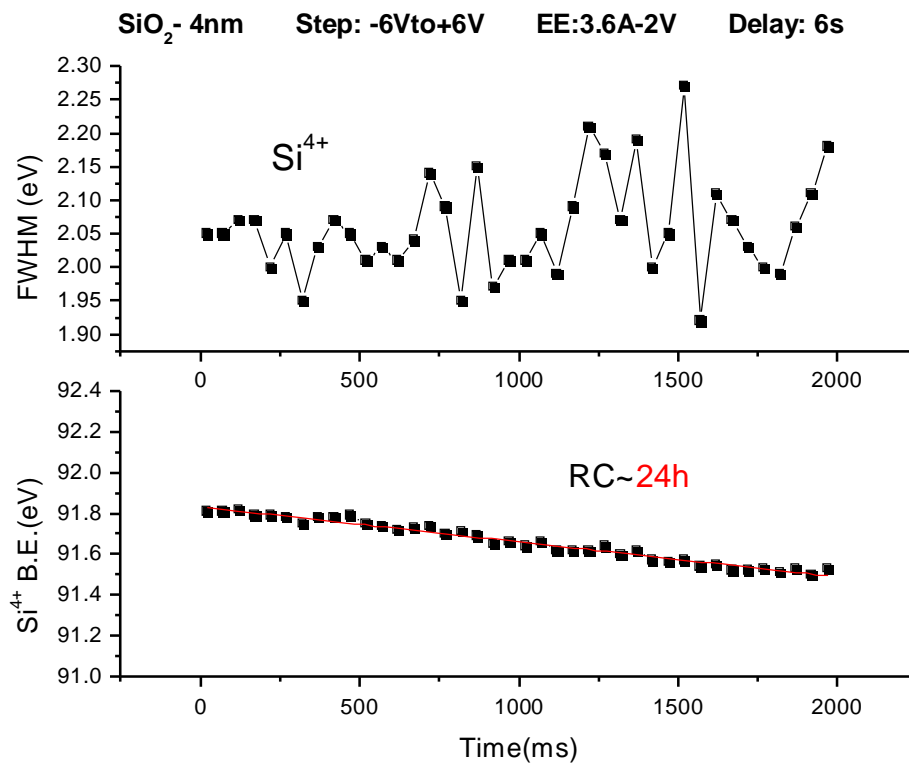
Figure 30. Shift of Si^{4+} peak maxima and the accompanying changes in FWHM. The sample is ~4 nm thick.

The change of peak position of the 4nm-oxide peak under the same experimental conditions as the previous sample is shown in Figure 30. It is visible from the above figure that decreasing the sample thickness induced a dramatic change in the time constant of the

oxide layer. Exponential fit of the charging curve gives a large RC constant of 24 hours, meaning that the 4-nm thick oxide layer practically does not charge in the given period. Moreover, the FWHM of the oxide peak does not display a significant change during the same period.

4.8. Voltage Dependence of Time Resolved Spectra

Upon increasing the amplitude of the voltage step, it was observed that the shifts due to charging were also magnified. However, the results of reversing the voltage steps on charging/discharging curves and time constants are not that straightforward. The overall response of the system is determined by execution and combination of internal charging mechanisms.

4.8.1. The Effects of Reversing the Polarity of Pulses

It is observed in numerous experiments that if the both of the step voltages have the same polarity, i.e. either positive or negative, reversing the polarity of the voltage pulses does not have a significant effect on neither the time constants nor the amplitudes of the corresponding shifts.

In Figure 31 below, two charging curves recorded under two different voltage pulses are shown. Both of the curves give a time constant of ~500ms upon exponential fitting indicating that the charging and discharging processes in this region proceed in similar time frames.
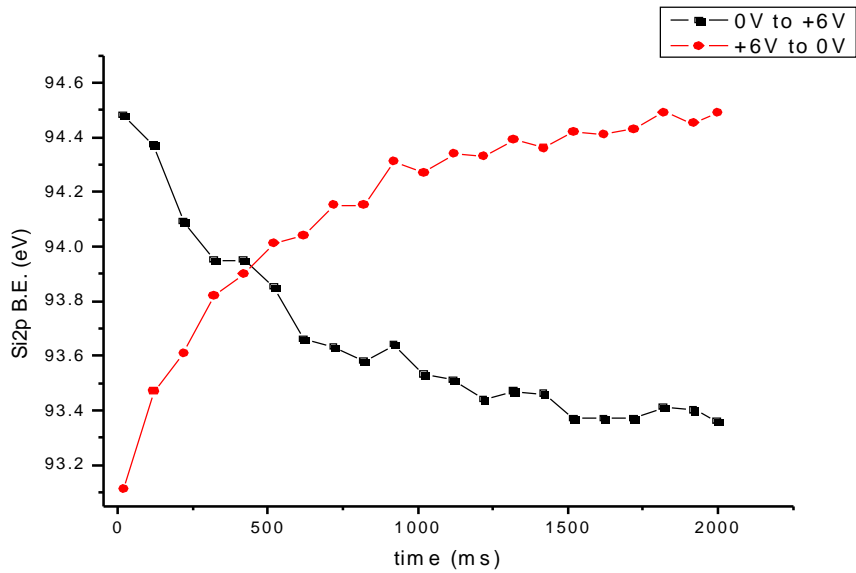
Figure 31. Charging and discharging curves for a 20-nm thick SiO_2 overlayer under 3.4A low energy electron emission. Voltage steps are indicated in the figure.

In Figure 32 below, the similarities of charging and discharging curves in the negative biasing region are displayed in the same graph for a thick silicon dioxide sample. The discharging behavior of the sample when going from -10V to zero potential is shown in (a). When going from -10V from 0V, it is shown in (b) that the sample charges with a similar time constant as in (a). Therefore so long as the charging takes place in the same region, i.e. positive or negative, the process proceeds through similar mechanisms in similar time periods and is reversible.
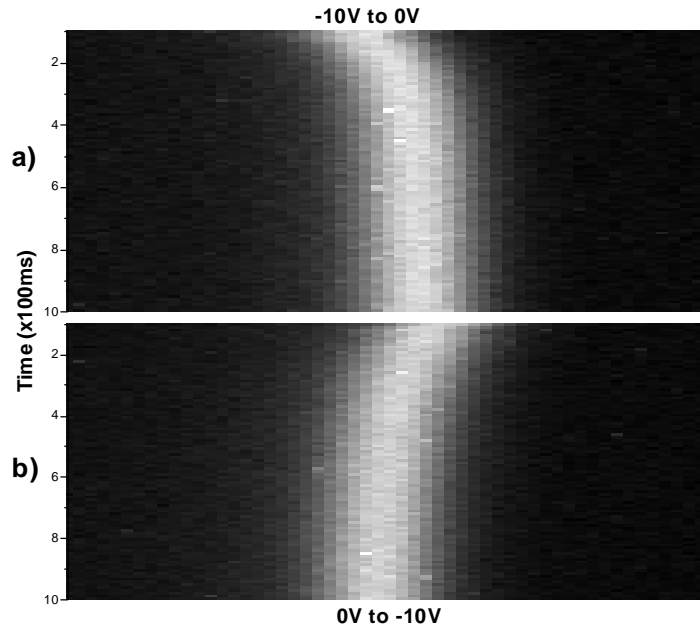
Figure 32. Si2p regions of a thick (ca.400 nm) SiO_2 layer showing the charging (b) and discharging (a) curves in the negative bias region.

However, due to differences in charging mechanisms of positive and negative charging, an asymmetrical charging behavior is observed upon the reversal of the bipolar voltage steps in the time resolved spectra. Figure 33 shows the situation in which a +10V to -10V pulse is applied to a 400nm-thick silicon dioxide to get the time resolved spectra in (a). The opposite step gives a spectra as in (b) in which the oxide Si2p peak maxima is more rapidly changing in time when compared to its counterpart in (a). This implies that discharging from a positively charged situation in (b) proceeds faster with the help of extra stray electrons than the process in (a) in which the sample is discharged from a negatively charged state.
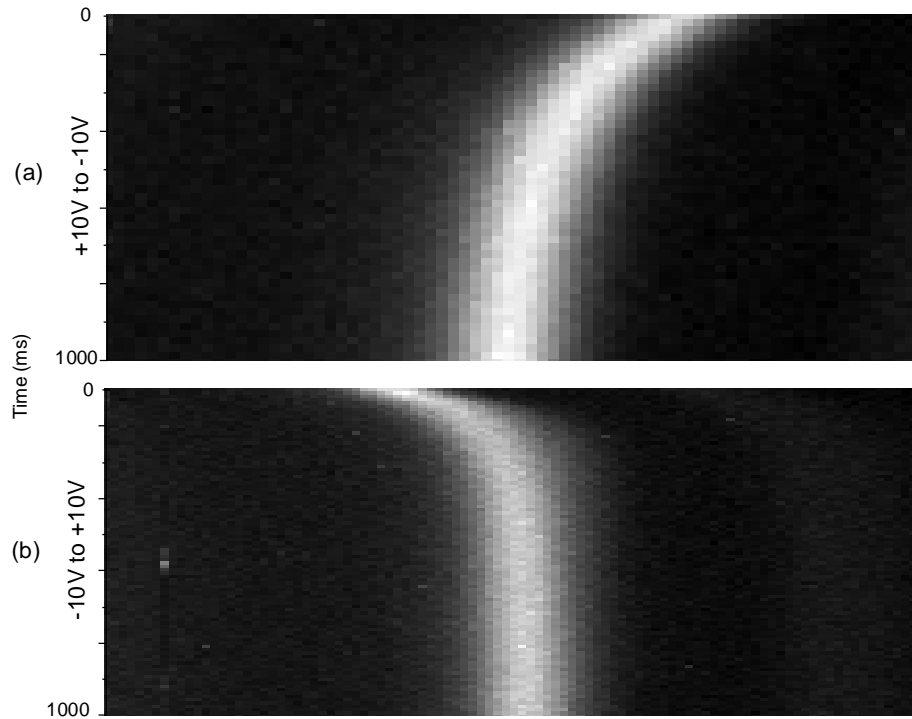
Figure 33. Reversal of the voltage step and the associated changes induced in the charging process of a thick silicon oxide layer. The current passing through the filament of the electron gun is 3.4A with no floating voltage applied.

4.9. Elucidation of Electrical Parameters of Surface Structures with External Biasing

4.9.1. Electrical Modeling of Surface Structures

Surface structures having sizes in nanometers are very important for many scientific and industrial applications. Thus, investigation of material and electrical properties of these structures have been an interesting topic for many scientists.[14,16,20,50,51] Most of these studies have employed the charging process where controlling it when necessary. Although the

discussions about charging phenomena in XPS date back to 1970's, its utilization in electrical measurements is rather new, yet very promising. However, in most of the cases it is good to have an electrical model of the system under analysis at hand. Instead of atoms, clusters and layers, an equivalent electrical circuit representing the actual sysyem is derived for simplicity. Due to its semi-conducting behavior, we have assumed that the bulk silicon has a finite resistance R with a capacitance C. However, SiO_2 which is deposited on top of the silicon underlayer, has a much larger resistance and capacitance. Therefore, the contribution of Si substrate to electrical parameters of the system is generally omitted throughout the measurements and calculations for simplicity and clarity.

As a starting point general electronic schematic of the Si/SiO_2 system is shown in Figure 34 below.
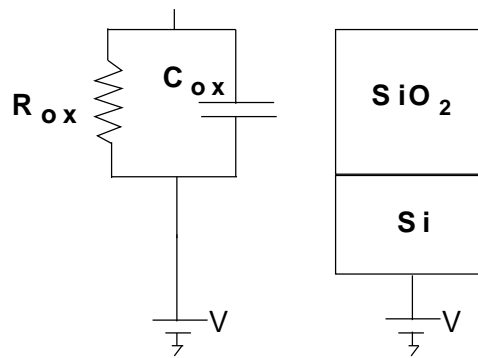
Figure 34. Electrical equivalent of Si/SiO_2 system

4.9.2. The Use of External Resistance

The effect of connecting an external resistance to the sample system on the observed binding energy shifts is analyzed by both conventional and time resolved XPS analysis.
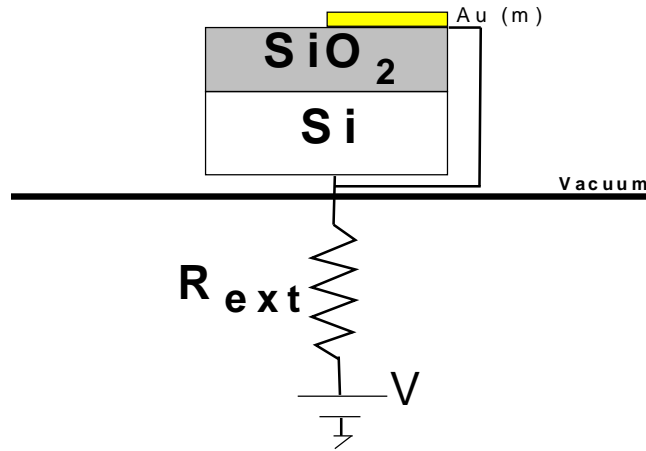
Figure 35. Connections showing the introduction of a series external resistance to the Si/SiO$_2$ system.

The biggest advantage of connecting an external resistor to the sample and investigating the overall response of the system under different external biases is the possibility of estimation of the internal resistance of the components, such as oxide overlayer in this case, that constitute the overall chemical system in a totally non-destructive and non-contact fashion.
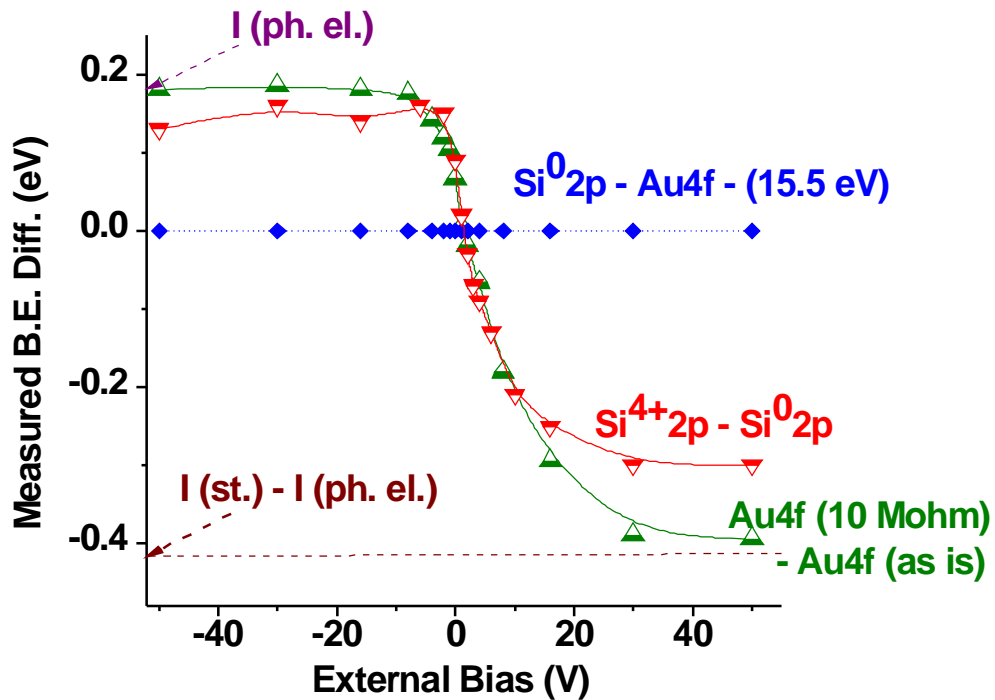
Figure 36. The measured binding energy difference between the Si2p peaks of the oxide layer (approximately 4 nm thick) and the silicon substrate plotted against the external voltage bias. The measured binding energy difference between the Au4f peaks with and without 10 MΩ external resistance is also shown in green. The binding energy difference between the Si2p of the substrate and Au4f does not change.

The schematic of the measurement setup is shown Figure 35. The difference of Au4f (10MΩ external resistance) and Au4f photoemission with no external resistance is shown in green. The resemblance of this charging curve to the curve drawn by taking the differences in Si2p photoemission of bulk silicon and the oxide creates the possibility of estimating the

internal resistance of the oxide layer as 8MΩ since the distance between two horizontal lines in the graph linearly changes with the resistance[52]. This value is comparable though not perfectly overlapping with a similar value of 0.83MΩ/nm reported in a previous XPS study[50]. As also seen from the graph, gold and bulk silicon do not exhibit a differential shift in binding energies with bias.

However, it must be noted that the resistance values derived with the procedure described above are good estimates of the actual photoresistance values rather than being the absolute value itself since the oxide is under X-ray and low energy electron exposure during the measurements.

4.9.3. External RC

Having estimated the resistance of the oxide layer, time resolved measurements are done in order to obtain a value for the time constant of the 4-nm oxide overlayer under investigation.
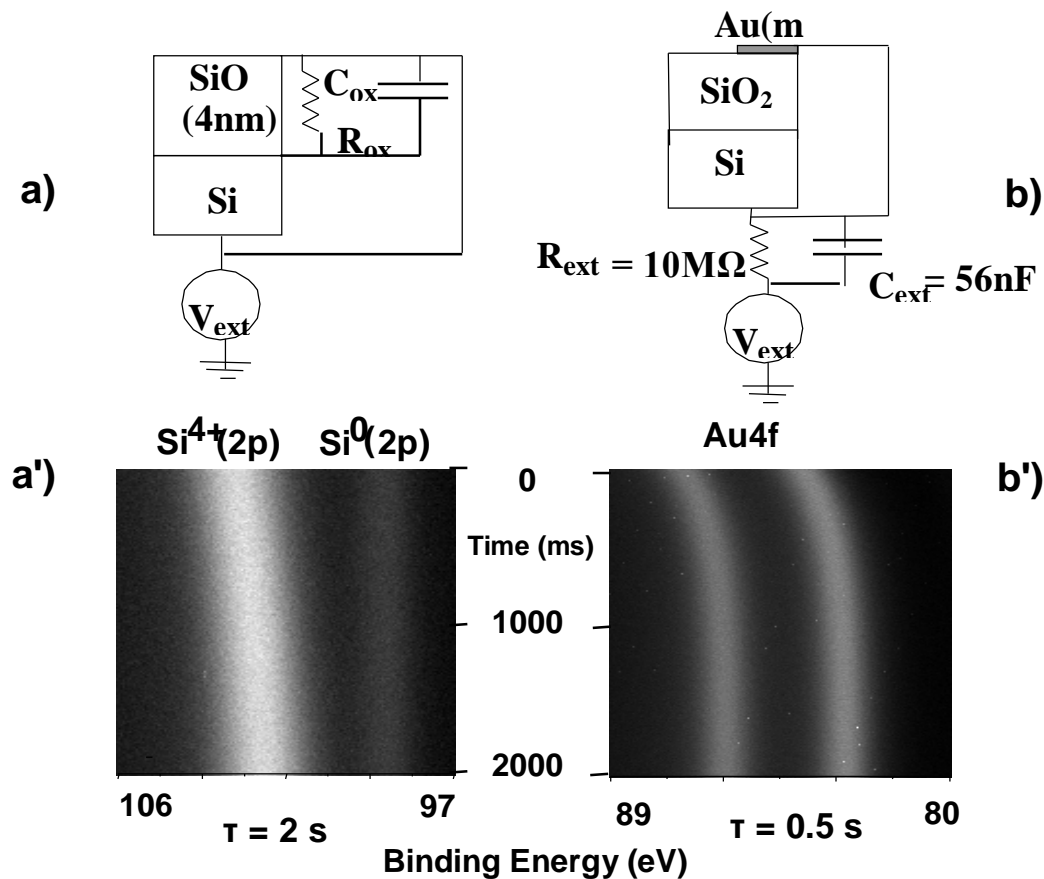
Figure 37. 200 time-dependent XPS spectra of the Si2p region for the SiO_2(4 nm)/Si system (a'), and the Au4f region of a gold metal strip connected to an external 10 Mohm series resistor and a 56 nF parallel capacitor (b'). The schematics of the two systems are also shown above in a and b. First order exponential fits give time constants of 2 and 0.5 s for the Si/SiO_2 and the Au(m) with the external RC circuit respectively.

When combined with the RC constant found from time resolved measurements which is seen in Figure 37, the capacitance of the 4 nm oxide layer is estimated to be around 250nF since the multiplication of 8MOhm with 250nF gives a product of 2000ms, i.e. the result obtained from the first order exponential fit of the shift in Si^{4+} peak maxima. An illustration

61

of how the oxide behaves like an electrical circuit element having a resistor and a capacitor connected in parallel is shown in Figure 37 a).

Moreover, the gold, being a perfect conductor, which normally does not exhibit time-dependent external bias induced shifts, is charged completely in the same fashion as the other naturally charging components such as the oxide layer by connecting an external series resistor and a parallel capacitor. A time constant of 0.5s is obtained from TRXPS which is in very good agreement with the theoretical value of 0.56s. The situation is illustrated in Figure 37 b') together with the equivalent circuit used in time resolved measurements shown in Figure 37 b). Thus, it was shown that by playing with the electrical parameters of the system, even the charging process of a perfect conductor like gold having very small resistance and capacitance (thus, a very small RC constant) values can be monitored by time resolved XPS as if it has already a detectable RC constant by its nature (eg. SiO_2).

4.10.   Simulation of Depth Dependent Sample Potential under External Stimuli

The depth dependent potential profile of a sample under external bias is simulated by combination of experimental and theoretical techniques. A 10nm-SiO_2, which is deposited on top of a Si substrate, is charged under external bias at different voltages and analyzed with XPS. A gold foil is also attached to the rod for referencing purposes. Si2p peak of the oxide is fitted to 10 individual peaks each of which are assumed to be coming from separate 1nm portions of the total 10nm-thick oxide overlayer. To determine the relative intensity ratios of the peaks, $I(d)=I_0\exp(-d/\lambda)$ is used, where d is the depth of the layer and λ is the attenuation

62

length of the photoelectrons in SiO_2, which is taken as 2.6 nm.[4] A typical Si2p peak consisting of 10 different peaks is shown below.
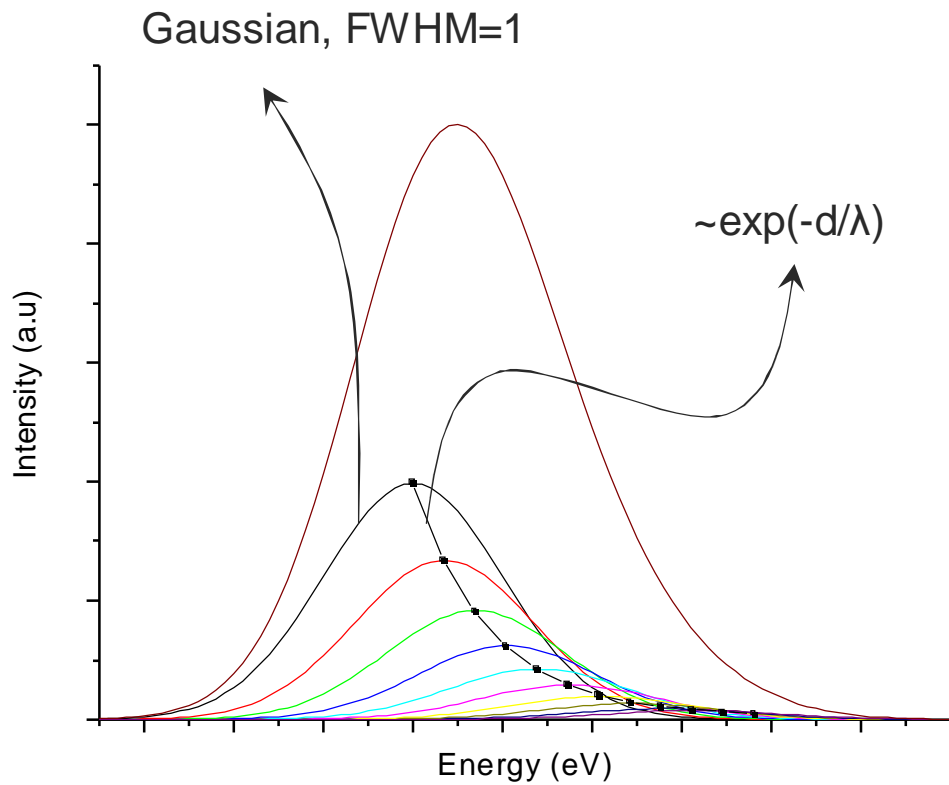
Figure 38. A simulation of a Si2p peak composed of 10 different smaller peaks. For practical purposes, the small peaks are assumed to be Gaussians of FWHM=1. The data points of the exponential decay curve specify the intensity ratios of the peaks but not necessarily the peak positions.

Si2p peaks collected at various external biases are fitted and the positions of the photoemission signals coming from different layers at a specific bias are determined as shown below.
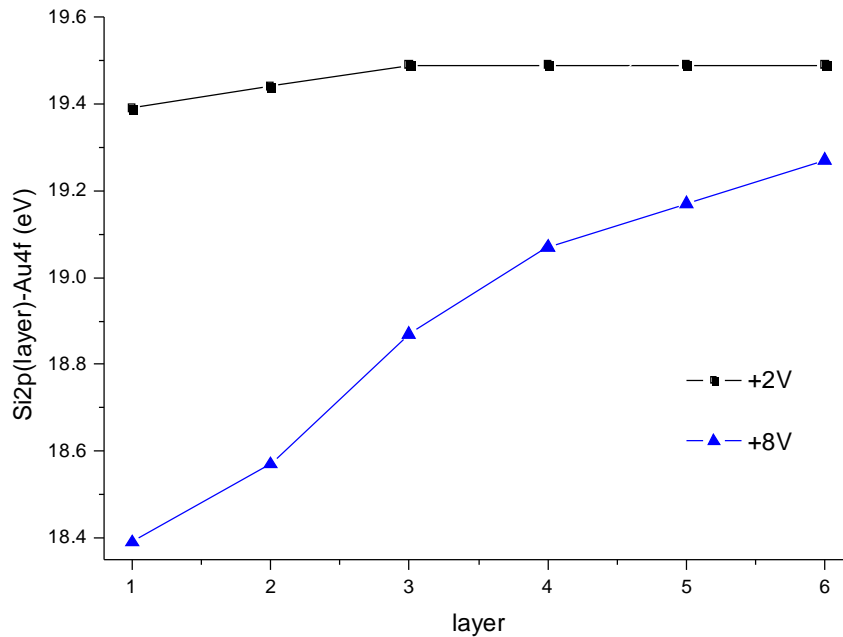
Figure 39. Si2p-Au4f differences belonging to outermost 6 layers at two different potentials are shown. Low energy electron emission (3.4A-4V) was turned on during the measurements.

It is noted from the figure above that the binding energy difference between the oxide and the gold peaks increase as the depth from the surface increases. Additionally, differences between the positions of the signals coming from different layers are amplified as the magnitude of the external bias is increased. These suggest that the surface is more negatively charged with respect to others and the effectiveness of the low energy electrons decrease as the distance from the surface increases. A potential gradient of 0.14V/nm at +8V is found from the graph above by simply dividing the potential drop across 6 nm by the corresponding depth. The values at other voltages can be found similarly. A qualitative model of the depth dependent sample potential is shown below.
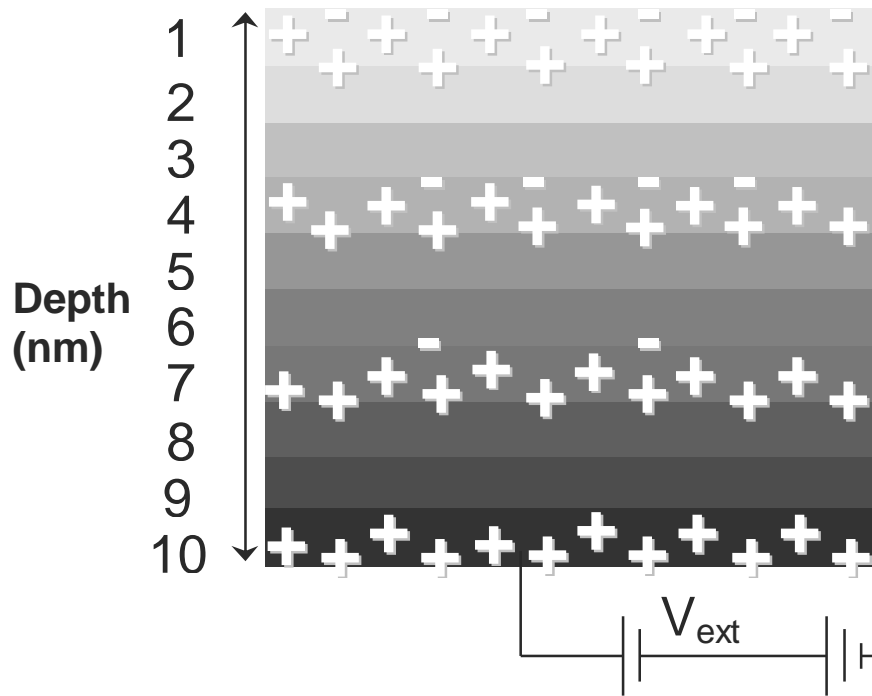
Figure 40. A model illustrating the potential profile of the top 10 nm of

a sample upon application of a positive bias.

To determine the current passing through the sample under external bias, a resistance is connected between the rod and the sample. The electrons, passing through the rod but not through the sample, are avoided by this internal resistance. The potentials of the layers are again determined by the same procedure explained above.
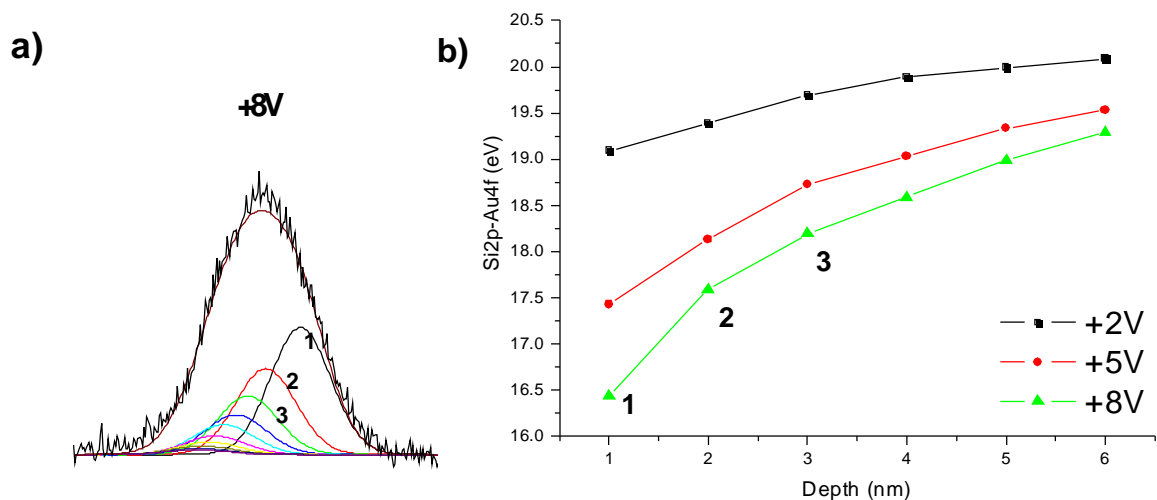
Figure 41. A Si2p peak and peak fitting results are shown in a). Relative Si2p peak positions in three different voltages with respect to gold in b). The photoemission coming from the first three layers under +8V external bias are marked as 1, 2, and 3.

Similar but clearer results are obtained in the case of internal resistance due to the fact that in addition to the resistance of the previous Si/SiO_2 system, an additional resistance of $1M\Omega$ also draws current and magnifies the binding energy shifts accordingly. The situation is summarized in the figure above together with an experimental Si2p peak decomposed into its constituents.

The layer that responds most to the change in external bias is the outermost layer as expected. The others display the same behavior but with less binding energy shifts as shown in the figure below. A shift of more than 4eV is observed in the top layer when going from grounded spectrum to the case when the sample is biased with +20V. This shows that the degree of neutralization caused by the low energy electrons is strongly affected by the application of external bias such that the sample attracts more electrons which penetrate

deeper into the sample starting from the outermost few nanometers as the magnitude of the positive potential is increased.
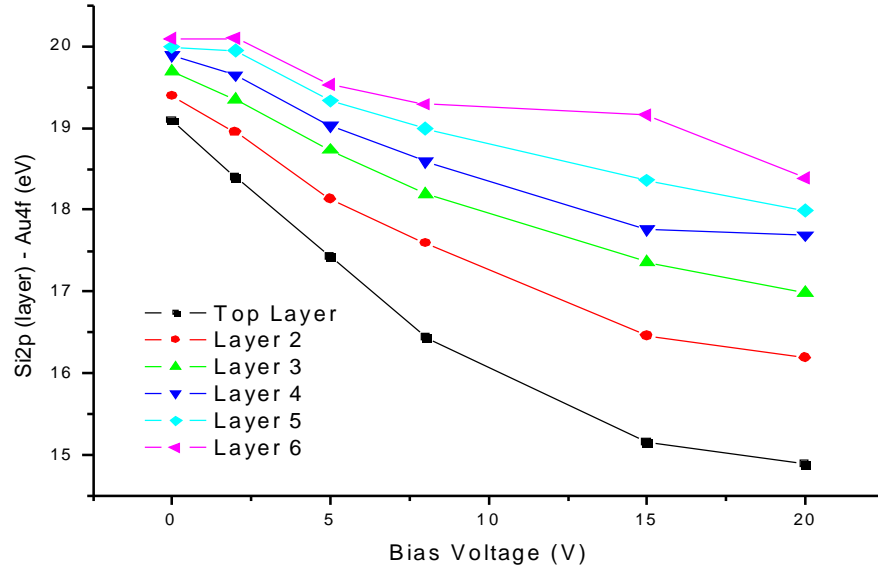
Figure 42. The binding energy shifts observed in each layer versus external voltage

5. CONCLUSIONS

The major contribution of this thesis work is the introduction of a novel technique in the analysis of surface structures by X-ray photoelectron spectroscopy, which allows the user to record two hundredth conventional XPS spectra in a period of one second with a time resolution of 5ms, which was of the order of 3-5 minutes in other XPS studies prior to this work.

This technique is used to monitor the charging process of a 400nm-thick SiO_2 layer in time. It is found that the previously known binding energy shifts of the oxide layer that are seen upon application of an external potential proceed exponentially in time. This shift in peak maxima are fitted to a first order exponential to find the charging constant (i.e. time constant/RC constant) of the material in question. With the application of an external resistance and additional time resolved XPS studies estimate resistance and capacitance values of SiO_2 overlayers are obtained. It is also shown that bulk gold which has a very small RC value that is probably much below our detection limits can also resemble the charging behavior of naturally charging materials upon connecting through an external RC circuit to the system to mimic the electrical parameters of these time dependent charging exhibiters, such as SiO_2.

The parameters that affect the charging behavior and time constants of the materials are studied extensively. It is found that the as the thickness of the oxide is increased, RC constant decreases. This relationship is thought to be associated with the capacitance value of a parallel plate capacitor $C = \varepsilon \dfrac{A}{d}$, ε being the dielectric constant, A being the area of the plate and d being the distance between two plates, such that as the d value increases, the capacitance decreases, so the RC product. Another parameter, delay period, is found to be

associated with the total amplitude of charging such that the more 'delayed' processes display larger binding energy shifts in time resolved spectra. Photoemission current is also found to be effective on the time constants such that a linear increase in the photoemission current caused an exponential decay in the values of the RC constants. This is attributed to the role of photoemission intensity on trapping/detrapping mechanisms. The introduction of extra low energy electrons to the system is found to increase the limits of charging while expediting the process especially in the negative charging case. Another important finding was the asymmetry observed in positive and negative charging zones. Both the amplitudes and the rates of charging are found to be different from each other in these two zones under similar experimental conditions. In other words, the amounts of charging shifts and the time constants are found to be varying when going from +10V to -10V and -10V to +10V. Reversal of the step voltage in either positive or negative regions without interfering with the other is however found to produce almost two mirror images in charging curves.

To extend the time resolved measurements beyond Si/SiO_2 and test the applicability of the method with other systems, gold as nanoclusters are deposited on top of SiO_2 layers with various thickness values and analyzed under TRXPS. It is shown that the method is fully applicable also in these hetero-systems. Although there are slight differences in the magnitude and the rate of the process, a similar charging behavior is observed in gold particles capped with C_{12}-thiols.

The use of external bias to identify two different forms of gold that exist together in the same sample, as nanoparticles and its bulk state, is demonstrated with the application of positive and negative bias to the sample to stimulate the external-bias-induced separation of

the Au 4f peaks which were otherwise seen as overlapped photoemission signals in the grounded spectrum.

6. References

[1] H. Hertz, Ann. Physik 31,983 (1887).

[2] A. Einstein, Ann. Physik 17,132 (1905).

[3] K. Siegbahn, et. al.,Nova Acta Regiae Soc.Sci., Ser. IV, Vol. 20 (1967).

[4] D. Briggs, M.P. Seah, *Practical Surface Analysis – 2nd ed.*, Vol.1, Wiley, 1996.

[5] M. P. Seah, W.A. Dench, *Surf. Interface Anal.*, 1, 2 (1979).

[6] A. Ishizaka, S. Iwata, *Appl. Phys. Lett.*, 36(1), 71-73, (1980).

[7] O. Birer, S. Sayan, S. Suzer, A. Aydinli, *J. Molecular Science*, 480, 611-614, (1999).

[8] B. Ulgut, S. Suzer, J.Phys. Chem. B 107, 2939 (2003).

[9] F.J. Himpsel, F.R. McFeely, A. Taleb-Ibrahimi and J.A. Yarmoff, Phys. Rev. B 38(9), 6084 (1988).

[10] J.B. Metson, *Surf. Ineterface Anal.,* 27, 1069-1072, 1999.

[11] T. Dickinson, A. F. Povey, P. M. A. Sherwood, *J. Elec. Spec. Rel. Phen.,* 2, 441-447, 1973.

[12] A. Cros, *J. Elec. Spec. Rel. Phen.,* 59, 1-14, 1992.

[13] W.M. Lau, J. Appl. Phys. 67 (3), 1 Feb. 1990.

[14] J.H. Thomas, C.E. Bryson, T.R. Rampalone, *J. Vac. Sci. Technol. B*, 6(4) 1081-1086, 1988.

[15] W.M. Lau, *Appl. Phys. Lett.,* 54(4), 338-340, 1989.

[16] H. Doron-Mor, A. Hatzor, A. Vaskevich, T. Van der Boom-Moav, A. Shanzer, I. Rubinstein, H. Cohen, *Nature*, 406, 382-385, 2000.

[17] R.T. Lewis, M.A. Kelly, J. El. Spec. Relat. Phenom., 20, 105, 1980.

[18] T. Dickinson, A.F. Povey, P.M.A. Sherwood, *J. Elec. Spec. Rel. Phen.,* 2, 441-447, 1973.

[19] T.L. Barr, "Studies in Differential Charging", *J. Vac. Sci. Technol. A*, 7(3), 1677-1683, 1989.

[20] N.J. Havercroft, P.M.A. Sherwood, *Surf. Interface Anal.,* 29, 232-240, 2000.

[21] S. Suzer, Anal. Chem., 75 (24), 7026-9, 2003.

[22] P.E. Larson, M.A. Kelly, J. Vac. Sci. Tech., A, 16, 3483, 1998.

[23] F. Karadas, G. Ertas, S. Suzer, J. Phys. Chem. B 108, 1515-1518 2004.

[24] N.J. Havercroft, P. M. A. Sherwood, Surf. Interface Anal., 29, 232, 2000.

[25] G. Ertas, U.K. Demirok, S. Suzer, Appl. Surf. Sci., In Press.

[26] K. Hirose, M. Yamawaki, K. Torii, T. Kawahara, S. Kawashiri, T. Hattori, Applied Surface Science 237, 411–415, 2004.

[27] Z.W. Deng, R.W.M. Kwok, W.M. Lau, L.L. Cao, Applied Surface Science 158, 58–63, 2000.

[28] S. Iwata, A. Ishizaka *J. Appl. Phys.* 79 (9), 6653-6713, 1996.

[29] F.R. McFeely, K.Z. Zhang, M.M. Banaszak Holl, S. Lee, J.E. Bender IV, *J. Vac. Sci. Technol. B* 14(4), 2824-2831, 1996.

[30] K.Z. Zhang, M.M. Banaszak Holl, *J. Phys. Chem. B,* 102, 3930-3935, 1998.

[31] H. Kobayashi, T. Kubota, H. Kawa, Y. Nakato, M. Nishiyama, *Appl. Phys. Lett.*, 73(7), 933-935, 1998.

[32] G.F. Cerofolini, C. Galati, L. Renna, *Surf. Interface Anal.*, 34, 577-582, 2002.

[33] R. Moreau, *The Computer Comes of Age: The People, the Hardware, and the Software*, translated by J. Howlett (Cambridge: MIT Press, 1984).

[34] Stan Augarten, *BIT By BIT: An Illustrated History of Computers* (New York: Ticknor & Fields, 1984).

[35] G.F. Cerofoni, L. Meda, *Springer Verlag*, New York, 1989.

[36] International Technology Roadmap for Semiconductors, 1999 Edition (Semiconductor Industry Association, Santa Clara, California, 1999).

[37] C. Wyon, Nuclear Instruments and Methods in Physics Ressearch B 186, 380-91, 2002.

[38] J. Turkevich, P.C. Stevenson, J. Hillier, *Faraday Discussions Chemical Society,* 11, 55, 1951.

[39] M.M. Alvarez, J.T. Khoury, T.G. Schaaff, M.N. Shafigullin, I. Vezmar, R.L. Whetten, *J. Phys. Chem. B*, 101, 3706-3712. 1997.

[40] S.R. Hall, W. Shenton, H. Engelhardt, S. Mann, *ChemPhysChem*, 2 (No.3), 184-186, 2001.

[41] S.L. Cumberland, F. Strouse, Langmuir, 18, 269-276, 2002.

[42] W. Cheng, E. Wang, J. Phys. Chem. B., 108(1), 24-26, 2004.

[43] M. Brust, M. Walker, D. Bethell, D. J. Schiffrin, R. Whyman, *J. Chem. Soc., Chem. Commun.* 801, 1994.

[44] G. Ertas, S. Suzer, Surf. Interface Anal., 36, 619-623, 2004.

[45] U. K. Demirok, G. Ertas, and S. Suzer, *J. Phys. Chem. B*, *108,* 5179-5181, 2004.

[46] O.L. Jr. Curtis, J.R. Srour, *J. Appl. Phys*, *48*, 3819, 1977.

[47] R.C. Hughes, *Phys. Re*V. *B*, *15*, 2012, 1977.

[48] T. Wang, T.E. Cheng, L.P. Chiang, C.H. Wang, N.K. Zons, C. Huang, *IEEE Trans. Electron De*V*ices*, *45*, 1511, 1998.

[49] C.J. Kang, G.H. Buh, S. Lee, C.K. Kim, K.M. Mang, C. Im, Y. Kuk, *Appl. Phys. Lett.*, *74*, 1815, 1999.

[50] H. Cohen, Appl. Phys. Lett,. *85*, 1271-73, 2004.

[51] H. Kobayashi, K. Namba, Y. Yamashita, Y. Nakato, T. Komeda, Y. Nishioka, J. Appl. Phys.**, *80*, 1578-1582, 1996.

[52] G. Ertas, U.K. Demirok, A. Atalar, and S. Suzer Applied Physics Letters [Submitted].